Chain Branching and Termination in the Low-Temperature Combustion of n-Alkanes: 2-Pentyl Radical + O-2, Isomerization and Association of the Second O-2

ARTICLE *in* THE JOURNAL OF PHYSICAL CHEMISTRY A · JULY 2010

Impact Factor: 2.69 · DOI: 10.1021/jp101159h · Source: PubMed

2 AUTHORS:

Rubik Asatryan
University at Buffalo, The State University …
51 PUBLICATIONS **366** CITATIONS
SEE PROFILE

Joseph W. Bozzelli
New Jersey Institute of Technology
277 PUBLICATIONS **5,269** CITATIONS
SEE PROFILE

Chain Branching and Termination in the Low-Temperature Combustion of *n*-Alkanes: 2-Pentyl Radical + O_2, Isomerization and Association of the Second O_2

Rubik Asatryan and Joseph W. Bozzelli*

Department of Chemistry and Environmental Science, New Jersey Institute of Technology, Newark, New Jersey 07102

Received: February 5, 2010; Revised Manuscript Received: May 24, 2010

Association of alkyl radicals with ground-state oxygen $^3\Sigma_g^+(O_2)$ generates chemically activated peroxy intermediates, which can isomerize or further react to form new products before collisional stabilization. The lowest-energy reaction (~19 kcal mol^{-1}) for alkylperoxy derivatives of C_3 and larger *n*-hydrocarbons is an isomerization (intramolecular H-atom transfer) that forms a hydroperoxide alkyl radical, and there is a ~30 kcal mol^{-1} barrier path to olefin plus HO_2, which is a termination step at lower temperatures. The low-energy-barrier product, hydroperoxide alkyl radical intermediate, can experience additional chemical activation via association with a second oxygen molecule, where there are three important paths that result in chain branching. The competition between this HO_2 + olefin termination step of the first O_2 association and the chain branching processes from the second chemical activation step plays a dominant role at temperatures below 1000 K. Secondary *n*-pentyl radicals are used in this study as surrogates to analyze the thermochemistry and detailed kinetics of the chemical activation and stabilized adduct reactions important to chain branching and termination. As these radicals provide six- member ring transition states for H-atom transfer between secondary carbons, they represent the detailed kinetics of larger alkane radicals, such as the common fuel components *n*-heptane and *n*-decane. Comprehensive potential energy diagrams developed from multilevel CBS-QB3, G3MP2, and CBS-APNO and single-level ab initio and density functional theory methods are used to analyze secondary 2-pentyl (*n*-pentan-2-yl) and interrelated 2-hydroperoxide-pentan-4-yl radical interactions with O_2. The thermochemistry and kinetics of the chemical activation and stabilized adduct reactions important to chain branching and termination are reported and discussed. Results show that the chain branching reactions have faster kinetics in this system because the barriers are lower than those observed in ethyl and propyl radical plus O_2 reactions; consequently, the branching is predicted to be more important. The lower barriers for branching result in less competition from the termination (HO_2 + olefin) path in this larger radical. Several nontraditional reaction channels not previously considered in the literature are identified. A pathway is suggested to explain the formation of a unique trioxane product observed experimentally.

1. Introduction

The interaction of triplet oxygen $^3\Sigma_g^+(O_2)$ with alkyl radicals and their alkylperoxy derivatives plays a critical role in practical combustion systems, namely, autoignition in homogeneous charge compression ignition (HCCI) and diesel engines and preignition (knock) in spark-ignited engines. The energized peroxy adducts generated from the association of alkyl radicals with an oxygen molecule typically have sufficient energy to react over several low-energy isomerization or elimination barriers before their collisional stabilization. These new isomers may also have an adequate energy to dissociate further to smaller and more stable products.

In an oxygen-rich environment, the intermediate hydroperoxide alkyl radicals produced from the peroxy radicals via an intramolecular hydrogen-transfer isomerization can associate with a second O_2 and undergo a set of second chemical activation reactions. These two association (oxidation) steps are partly described for C_2-C_4 molecules (reactions of ethyl, *n*-propyl, *i*-propyl, primary *n*-butyl, and dimethyl ether radicals + O_2)[1−14] and are currently considered for inclusion in advanced kinetic mechanisms for larger hydrocarbons. However, the specificity of larger hydrocarbons with their "more diverse chemistry" is challenging for the study of more relevant molecular models.

Reactions of *n*-pentyl radicals C_5H_{11}-1, C_5H_{11}-2, and C_5H_{11}-3 (denoted for brevity as PN-1J, PN-2J, and PN-3J, with J being the radical site, vide infra) with an extended linear carbon backbone can be considered as significant surrogates for the diverse oxygenation processes in the larger fuel component hydrocarbons such as *n*-heptane and *n*-decane. For instance, the *n*-pentan-2-peroxy radical generated from 2-pentyl radical association with molecular oxygen can undergo several intramolecular isomerization (H-atom transfer) reactions with the peroxy radical site through six- and seven-member cyclic structures with low ring strain, leading to different products in need of mechanism development. Oxidation of *n*-pentane has been studied by several researchers, and general features in product distributions are reported.[15−19] A variety of products are observed, including cyclic ethers and bifunctional products detailed by Wijaya, Sumathi, and Green.[9] Notably, a significant amount of pentyl hydroperoxides, dihydroperoxides, diols, and ketohydroperoxide are observed with low-temperature (100 °C) oxidation of liquid-phase *n*-pentane.[19]

This study details the potential energy surfaces (PES) of the two oxygenation steps for the secondary *n*-pentyl radical (PN-

* To whom correspondence should be addressed. E-mail: bozzelli@njit.edu.

10.1021/jp101159h
Published on Web 07/06/2010

2J) with triplet oxygen $^3\Sigma_g^+(O_2)$, namely, (i) the association, isomerization, elimination, and other product formation reactions from interaction of PN-2J with O_2 and (ii) the association reaction of an oxygen molecule with the hydroperoxide alkyl isomer PN-2Q4J, $CH_3CH(OOH)CH_2CH^{\bullet}CH_3$, generated from the lowest-energy intramolecular H-transfer (isomerization) process in the first O_2 association step. Some concepts of this study have been reported at several combustion and kinetic forums.[20] Here, we provide a thorough version of the work.

The primary focus of this study is on the second O_2 association step (reaction of PN-2Q4J + O_2); however, we found several changes resulting from the larger hydrocarbon backbone in the reaction thermochemistry and kinetics of the first oxygenation association system to be substantial. Consequently, several reactions of the initial PN-2J + O_2 association were also studied. In particular, lower barrier pathways in the pentyl system were compared with the similar chemical activation reactions of primary and secondary propyl radical reactions.

The two-step O_2-association reaction system is important to ignition and oxidation of *n*-alkane fuels at low and moderate temperatures where the reverse dissociation channels have not yet become dominant. This issue is currently receiving common recognition. Recent experiments of Craig Taatjes and coworkers[21] at temperatures of 586−828 K and pressures of 6.5−20.3 bar have unequivocally confirmed the need to include chain branching steps. Subsequent to our initial theoretical predictions on the *n*-pentyl secondary radical oxygenation reactions,[20] it has been experimentally shown, for the first time, that low-temperature chain branching from the addition of the second oxygen to a large hydroperoxy radical such as cyclohexyl plays a central role at the pressures of practical combustors, along with the "formally direct" chemical activation pathways. We feel that theoretical studies on the larger systems are essential for the explanation of the diversity of low-temperature processes in the oxidation of hydrocarbons.

We present detailed thermochemistry, reaction pathways, and kinetics for the chemical activation and dissociation of stabilized adducts in the sequence of two oxygenation steps on the 2-pentyl radical (namely, reaction systems PN-2J + O_2 → PN-2QJ → PN-2Q4J and PN-2Q4J + O_2 → Products). We have analyzed the important chain branching and termination channels, which are both pressure- and temperature-dependent.

2. Computational Methods

The diversity of stationary points on the PES of interacting systems was first determined using moderate-level B3LYP/6-31G(d) density functional theory, which is reasonable in expense and considered to result in correct geometry of equilibrium and transition-state structures.[25] The B3LYP method combines the nonlocal Hartree−Fock exchange functional along with the corrective terms for the density gradient developed by Becke[22a] with the correlation functional by Lee, Yang, and Parr.[22b]

To obtain more accurate relative energies and structures, the complete basis set QB3 model chemistry, which includes more refined CCSD(T) calculations, was utilized.[23] The CBS-QB3 method is shown[7] to be in excellent agreement with the QCISD(T) results of DeSain et al.[5] on stationary point energies of the *n*-propyl + O_2 reaction system and with the dissociation energies of alkylperoxy radicals evaluated by Knyazev and Slagle (vide infra).[24]

The CBS-QB3 method uses the B3LYP functional for geometries and frequencies and combines the results of several electronic structure calculations and empirical terms to predict molecular energies to around 1 kcal mol^{-1} accuracy.[23] This is a relatively low-cost complete basis set method. Geometries and frequencies are calculated at the B3LYP/6-311G(2d,d,p) level. This basis set denoted originally as the CBSB7 basis includes 2d functions on the second-row elements, a d-polarization function on the first row, and an additional p-polarization function on hydrogen atoms. This p-polarization is included[23] to improve transition-state structures for hydrogen-transfer reactions (NB!). Two additional calculations are used in the CBS-QB3 method to approximate higher-order contributions, MP4(SDQ)/6-31+G(d(f),p) and CCSD(T)/6-31+G†). The CCSD(T) is considered to improve accuracy over the QCISD(T) method, especially for spin-contaminated radicals.[23] The 6-31G† basis is a modification of the 6-31G(d,p) basis obtained combining the 6-31G sp functions with the 6-311G(d,p) polarization exponents. There is also a correction for spin contamination (proportional to $\langle S^2 \rangle$) and a size-consistent higher-order empirical correction.

Spin contamination of the open-shell systems in this study was small as judged by the corresponding $\langle S^2 \rangle$ expectation values. In unrestricted B3LYP calculations, $\langle S^2 \rangle$ values for radicals were less than 0.76 before and 0.75 after spin annihilation. For the transition states, $\langle S^2 \rangle$ was larger (∼0.84). However, all values of $\langle S^2 \rangle$ were ≤0.755 after spin annihilation. Spin contamination in CBS-QB3 was also small ($\langle S^2 \rangle$ less than 0.78).

Expectation values were ≤2.05 for triplet species. To avoid spin contamination in some species, a restricted CCSD(T) analysis is preferred over an unrestricted wave function.

The CBS-QB3 method also has an advantage of utilizing the geometry and frequencies calculated at the same level of theory, namely, B3LYP/6-311G(2d,d,p), which is important for correct localization of TS structures along with the other benefits of the CBS-QB3 method in the prediction of correct barrier energies and geometry.[25] Final results presented here (on figures) are at this composite level of theory unless otherwise stated. For some specific structures, namely, the biradical and zwitterionic systems, we have additionally employed QCISD/6-31G(d,p), MP2/6-311++G(2df,p), and B3LYP/6-311++G(2df,p), single and G3MP2 and CBS-APNO multilevel methods with full geometry optimization in each case.

Transition states are characterized as having only one negative eigenvalue of Hessian (force constant) matrices. The absence of imaginary frequencies verifies that structures are true minima at their respective levels of theory. Intrinsic reaction coordinate (IRC) calculations were performed at the B3LYP/6-31G(d) level to ensure the connectivity of stationary points. In addition, the final point geometries at both sides of the TS were reoptimized at the CBS-QB3 level to proper minima. All DFT and ab initio calculations were performed using the Gaussian 03 suite of programs.[26]

Notation. Abbreviated names are employed for larger species, such as PN-2J, PN-2QJ, and PN-2Q4J for radicals C_5H_{11}-2, $CH_3CH(OO^{\bullet})CH_2CH_2CH_3$, and $CH_3CH(OOH)CH_2CH^{\bullet}CH_3$, correspondingly, where Q stands for an OOH group and J is a radical center. Digits indicate the position of the backbone atom, while letters and symbols describe attached substituents or hybridization (for example, * is a double and # represents triple bonds). Alpha (α), beta (β), gamma (γ), and delta (δ) denote positions of carbon atoms relative to C(2). This notation simplifies the managing of similar reaction schemes of homologous hydrocarbons in kinetic models which often contain only numbers or nondescriptive symbols. Replacement of a prefix, for example, PN- to BU-, HX-, HP-, DC-, and so forth, can represent analogous reactions for butane, hexane, heptane, and decane derivatives, respectively. The notations of TS-if-j and

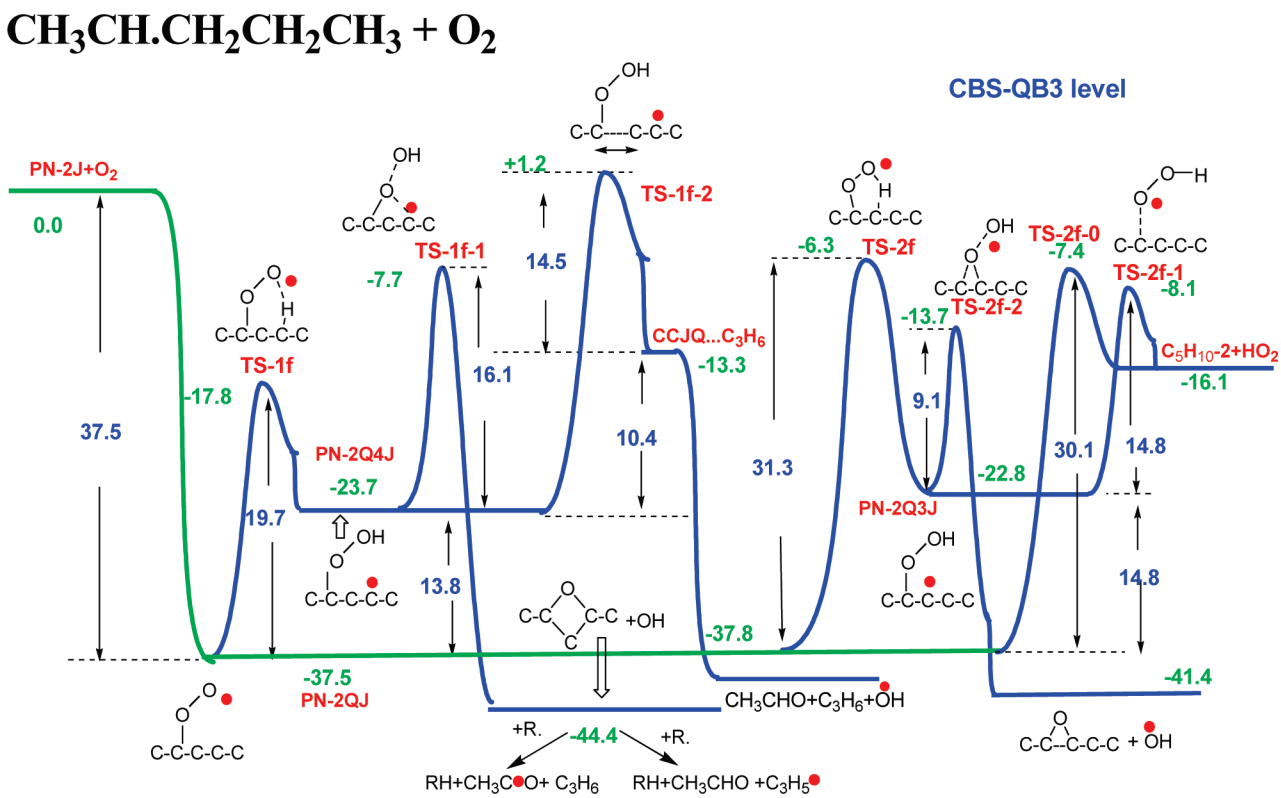

Figure 1. Enthalpy diagram of chemical activation pathways at first O_2 addition to the 2-pentyl secondary radical (*n*-pentan-2-yl or C_5H_{11}-2, denoted here as PN-2J) calculated at the CBS-QB3 level.

TS-is-j are used for transition states of the first O_2 and the second O_2-addition reactions, respectively.

3. Results and Discussion

Enthalpy diagrams for the association of O_2 with the 2-pentyl radical (the first oxygenation step) and for the hydroperoxide-*n*-pent-2-yl radical (second oxygenation step) are presented in Figures 1 and 2, correspondingly. Full optimized geometries are provided as Supporting Information (Table S1 and Table S2). The general features of first association reactions of the *n*-pentyl secondary radical are somewhat known from the literature on lower carbon number homologues (cf., Figure 1). The further association−transformation pathways from the *n*-pent-2-yl-4-hydroperoxide radical formed in the first association step reacting with O_2 are more complex and are less intuitive from conventional hydroperoxide and peroxy radical chemical reaction literature or perception (vide infra, Figure 8).

To the best of our knowledge, several of the reaction schemes that we present are new reaction types which occur only when large hydrocarbon backbones are involved. The results are discussed in comparison with the key steps involved in the O_2 association with the 2-pentyl radical below.

3.1. Association of the 2-Pentyl Radical with the First O_2 Molecule. The CBS-QB3 calculations suggest that the adduct 2-pentyl peroxy radical (PN-2QJ) formed by the addition of an O_2 molecule to the radical center of $CH_3CH^{\bullet}CH_2CH_2CH_3$ (PN-2J) has an energy excess (well depth) of 37.5 kcal mol^{-1} (see Table 1).

$$\text{PN-2J} + O_2 = \text{[PN-2QJ]*}$$

This value is in close agreement with the evaluated 37.6 kcal mol^{-1} experimental data of Knyazev et al.[24] for the simplest secondary *iso*-propylperoxy radical, consonant with the CBS-QB3 calculations performed by Hadad's group for this secondary system.[7] It is somewhat deeper than the well depth for the *n*-propylperoxy radical (36.1 kcal mol^{-1}).[24] The excess of internal energy upon formation of the activated peroxy radical can initiate several isomerization/transformation processes, as shown in Figure 1, before stabilization with the bath gas occurs.

The potential energy surface for the peroxy radical (PN-2QJ) includes several low-energy intramolecular transformation channels:

(A) Transfer of the β-hydrogen atom from the C(4) carbon to the peroxy radical center (intramolecular H-abstraction) via a six-member ring transition state TS-1f.

$$\text{[PN-2QJ]*} = \text{PN-2Q4J}$$

The barrier for this reaction (19.7 kcal mol^{-1}) is the lowest barrier reaction path and is located 17.8 kcal mol^{-1} below the entrance channel energy.

The resulting hydroperoxy radical PN-2Q4J can undergo dissociative four-member ring closure (16.1 kcal mol^{-1} barrier) to a *sym*-dimethyloxetane structure through the TS-1f-1 transition state with elimination of the OH radical. Alternatively, PN-2Q4J can react through a higher decomposition barrier to the acetaldehyde, propene, and OH radical product set via transition state TS-1f-2.

$$\text{PN-2QJ} = \text{2,4-dimethyloxetane} + \text{OH}$$

(two steps with an overall barrier of 29.8 kcal mol^{-1})

TABLE 1: Characteristic Stationary Point Parameters of the PES *2*-Pentyl + O_2 System Calculated at the CBS-QB3 Composite Level

system	H(298 K) au	ΔH^a kJ mol^{-1} (kcal mol^{-1})	$\sum S$(298 K) cal mol^{-1} K^{-1}	ν_i^b cm^{-1}
PN-2J + O_2	−346.804875	0.0 (0.00)	134.6	
PN-2QJ	−346.864697	−157.1 (−37.54)	94.6	
TS1-f	−346.833286	−74.7 (−17.83)	88.0	i1677.3
PN-2Q4J	−346.842591	−99.1 (−23.70)	94.97	
TS1-f-1	−346.817056	−32.0 (−7.64)	95.0	i731.7
TS-1f-2	−346.802981	5.1 (1.19)	96.6	i399.1
TS2-f	−346.814868	−26.2 (−6.27)	89.2	i2152.3
PN-2Q3J	−346.841185	−95.3 (−22.78)	98.9	
TS2-f-2	−346.826660	−57.2 (−13.67)	97.4	i668.5
TS2-f-0	−346.816823	−31.4 (−7.50)	93.0	i1034.9
TS2-f-1	−346.817689	−33.6 (−8.04)	96.3	i488.1

[a] Relative to entrance channel enthalpies. [b] Imaginary modes of transition states.

$$\text{PN-2QJ} = CH_3CHO + C_3H_6 + OH$$

(two steps with an overall barrier of 38.7 kcal mol^{-1})

(B) Intramolecular H-atom transfer can also occur at the primary α- and γ-sites (via five- and seven-member ring TSs, respectively), not illustrated in Figure 1. The barrier for a H-atom transfer through an extended (seven- to eight-member ring) TS is close to that of the six-member ring reactions[8] but has a lower pre-exponential factor. H-abstraction at the secondary C(3) α-position requires a substantially higher barrier of 31.3 kcal mol^{-1} (TS-2f).

(C) Abstraction of the secondary α-hydrogen atom, connected to C(3) via TS-2f leads to the formation of a PN-2Q3J intermediate radical. The reverse reaction through TS-2f has a significant (16.5 kcal mol^{-1}) barrier of activation, which is much higher than the analogous reverse reaction in the case of β-H-transfer (5.9 kcal mol^{-1} vide infra).

$$\text{PN-2QJ} = \text{PN-2Q3J}$$

We note that this H-transfer barrier is ∼4 kcal mol^{-1} lower than that in the *iso*-propylperoxy system (Table 3) and is approaching the competing barrier for molecular elimination of HO_2. Reactions of this PN-2Q3J isomer are discussed below.

(D) Reaction of the the PN-2QJ peroxy radical via concerted (direct) molecular elimination of HO_2 forms an olefin from either the adjacent primary or the internal C(3) sites, where barriers (TS-2f-0) are ∼30 kcal mol^{-1} relative to the stabilized adduct PN-2QJ.

$$\text{PN-2QJ} = HO_2 + \text{PN-2*} \qquad (\text{2-pentene}, C_5H_{10}\text{-2})$$

These molecular elimination reactions to olefin + HO_2 products are, in fact, chain termination processes at low temperatures due to the reaction of two HO_2 radicals to form $H_2O_2 + O_2$ (we note that H_2O_2 is a central component in higher-temperature combustion processes governing the second ignition stage).

The intramolecular H-atom transfer process from a primary α-site has a several kcal mol^{-1} higher barrier than TS-2f, resulting from the stronger primary C−H bond and smaller pre-exponential factor resulting from loss of an additional rotor; it is not included in the PE diagram for clarity.

Isomerization via the seven-membered transition state (formation of PN-2Q5J) has a small effect on the overall reaction kinetics due to the lower pre-exponential factor resulting from entropic effects.

The lowest barrier in this reaction system corresponds to the transition state TS-1f (19.7 kcal mol^{-1}), leading to hydroperoxide alkyl radical PN-2Q4J; however, further reaction of this intermediate has slightly higher barriers to product formation via TS-1f-1 and TS-1f-2 (Figure 1, Table 1). While the H-transfer reaction has a relatively low forward reaction barrier, the reverse isomerization has an even lower barrier of ∼5.9 kcal mol^{-1} but a lower pre-exponential factor; overall, the reverse reaction is faster than the forward at low temperatures. The low forward and reverse barriers under combustion conditions can result in a near equilibrium for PN-2QJ and the PN-2Q4J hydroperoxide alkyl radical. As a result, PN-2Q4J can readily undergo association with a second O_2 molecule (second oxygenation step), forming an activated hydroperoxide pentylperoxy radical PN-2Q4QJ, opening a variety of new reaction pathways.

The PN-2Q4J radical can also undergo a β-scission (βsc) reaction, cleaving the 2,3 carbon−carbon bond and forming propene + $CH_3C^{\bullet}H(OOH)$ radical, which rapidly decomposes to $CH_3CH(=O)$ + OH. While the overall reaction forming the propene, acetaldehyde, plus OH is exothermic by 14 kcal mol^{-1}, the βsc TS to the olefin does not see the carbonyl π-bond formation and effectively forms the hydroperoxide radical as an unstable intermediate; this step is 19 kcal mol^{-1} endothermic and has a barrier of 27 kcal mol^{-1}. The βsc elimination of a methyl H atom to form 2-hydroperoxide pentene has a barrier of 39 kcal mol^{-1}. This carbon chain cleavage is important in the larger alkyl hydrocarbons, where it is usually not considered in the peroxy chemistry.

(E) Decomposition of the PN-2Q3J intermediate (H-atom transfer isomer of PN-2QJ) involves two main paths, (a) the dissociative ring closure via transition state TS-2f-2 through the formation of a three-membered ring structure (2-methyl-3-ethyloxirane) and OH radical and (b) β-scission to HO_2 and pentene-2 (TS-2f-1). Formation of PN-2Q3J has a 31.3 kcal mol^{-1} barrier and is not an important step at low temperatures.

$$\text{PN-2Q3J} = \text{2-methyl-3-ethyloxirane} + OH$$

$$\text{PN-2Q3J} = HO_2 + \text{PN-2*}$$

3.2. Addition of a Second O_2 to the PN-2Q4J Intermediate Hydroperoxide Alkyl Radical. Reaction PN-2Q4J + O_2 → [PN-2Q4QJ]* → Products. The potential energy diagram of the second oxygenation step, namely, the association of PN-2Q4J hydroperoxy radical intermediate with the second oxygen molecule, is more complex. Figure 2 demonstrates only those

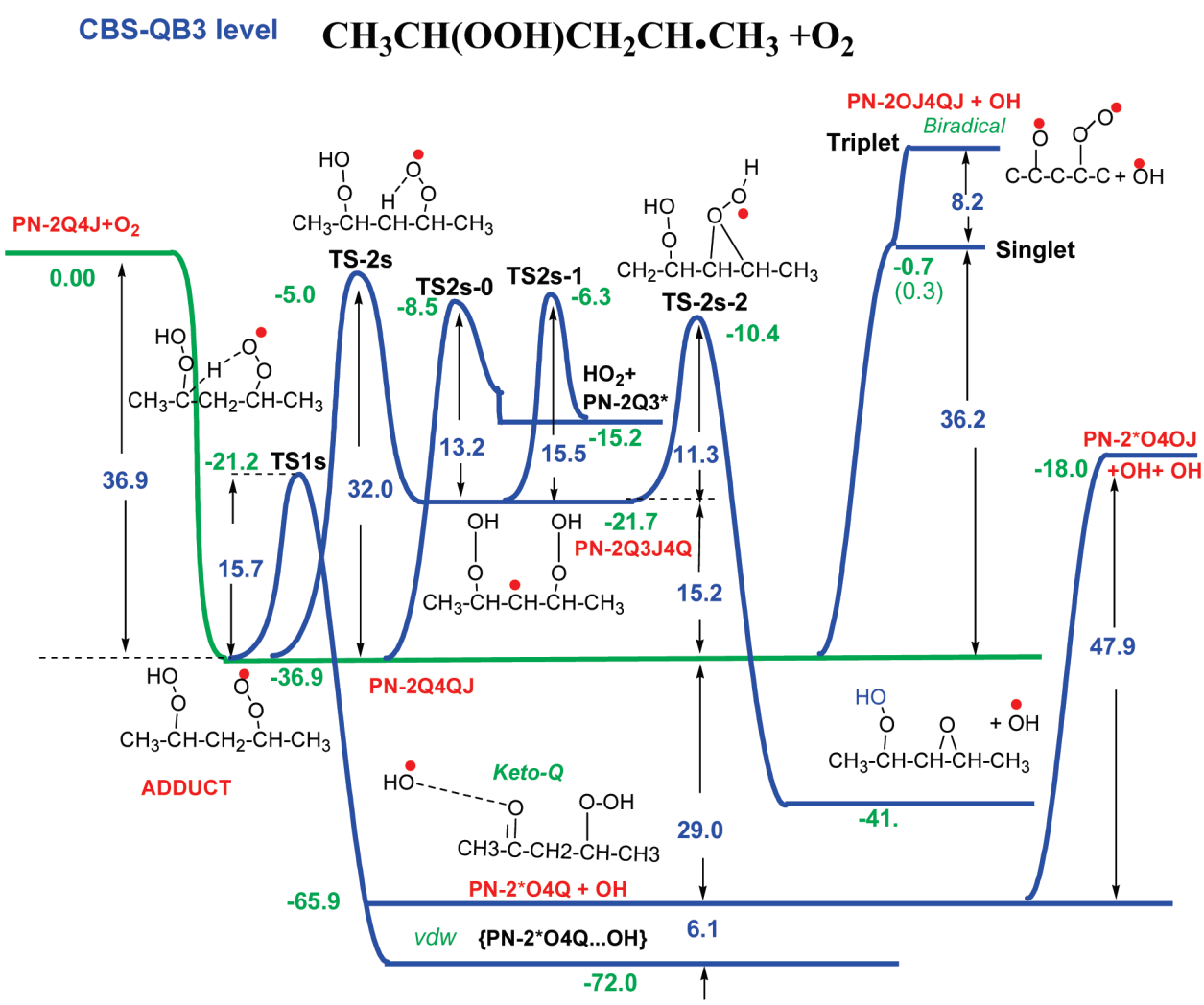

Figure 2. Fragment of the PES second oxygenation (chemical activation) reaction; addition of O_2 to 2-hydroperoxide-*n*-pentan-4-yl intermediate radical (PN-2Q4J + O_2) generated from the first oxygenation step, calculated at the CBS-QB3 level.

activation pathways, which we have included in kinetic analysis of this study (vide infra). A more complete version of this PES, including several novel, nontraditional pathways with highly interesting (new) transition states, will be considered in section 5. Table 2 lists characteristics of the stationary points and thermochemical parameters related to this second activation processes.

The energy of the chemical activation (well depth) for the second oxygenation step as is illustrated in Figure 2 is 36.9 kcal mol^{-1}; this is 0.6 kcal mol^{-1} lower than the well depth for a similar path in the first oxygenation step. There are several low-energy chain branching and termination pathways and a number of higher-energy paths with very intriguing intermediates on this energetic hypersurface. There are three important low-barrier channels on the PES of 2-pentyl radical involving energized [PN-2Q4QJ]* and a stabilized PN-2Q4QJ adduct leading to chain branching (Figure 2).

(A) Ketohydroperoxide Channel. The lowest-energy process for the second activation step is an intramolecular H-transfer reaction from the carbon atom bonded to the peroxide group carbon to the oxygen of the peroxy radical via transition state TS1s (Figure 2, Table 2). The barrier is 21.2 kcal mol^{-1} below the entrance channel, and this path forms a highly unstable intermediate with a radical center localized on the carbon atom attached to the hydroperoxide group. The radical is expected to dissociate with little or no barrier (less than several kcal mol^{-1}) via the formation of a strong carbonyl double bond in the ketohydroperoxide intermediate, $CH_3C(=O)CH_2CH(OOH)$-CH_3 (structure denoted as keto-Q in Figure 2). The energy gain, relative to the H-shift TS, is 56 kcal mol^{-1}; this is more than sufficient to cleave the weak RO−OH bond (~45 kcal mol^{-1}) in a hydroperoxide under conditions of chemical activation. The exothermicity relative to the stabilized PN-2Q4QJ adduct is 29 kcal mol^{-1} (see the bottom of Figure 2). The product set is additionally stabilized through the formation of a van der Waals complex between isolated products. Enthalpy of this vdW complex formation is ~6 kcal mol^{-1} without taking into consideration basis set superposition error (BSSE) correction, which is expected to be negligible at the composite CBS-QB3 calculation level.

The reaction converting the stabilized peroxy adduct to the (keto-Q + OH) product set has a barrier of only 15.7 kcal mol^{-1} (TS1s), 21.2 kcal mol^{-1} below the entrance channel.

This reaction produces a chemically activated [$CH_3C(=O)$-$CH_2CH(OOH)CH_3$]*, ketohydroperoxide (keto-Q*), which is stabilized by 44.7 kcal mol^{-1} relative to the intramolecular H-transfer TST barrier, TS1s. The isolated product set is stabilized even more, by 65.9 kcal mol^{-1} relative to the PN-2Q4QJ + O_2 entrance channel. The activated ketohydroperoxide can readily cleave the remaining weak RO−OH bond (47.9 kcal mol^{-1}; see Figure 2), forming a second OH radical plus a ketoalkoxy radical. The net overall reaction of this H-transfer

TABLE 2: Calculated at the CBS-QB3 Level Stationary Point Parameters of the PES 2-Hydroperoxy-4-*n*-pentyl + O_2

structure	H(298 K) au	$\sum\Delta H^a$ kJ mol^{-1} (kcal mol^{-1})	$\sum S$(298 K) cal mol^{-1} K^{-1}	ν_i^b cm^{-1}
PN-2Q4J + O_2	−497.003742	0.0 (0.00)	143.95	
PN-2Q4QJ	−497.062586	−154.5 (−36.92)	106.15	
TS1-s	−497.037560	−88.8 (−21.22)	98.34	i1643.3
PN-2*O4Q + OH	−497.108268	−274.4 (−65.59)	140.59	
PN-2*O4OJ + OH + OH	−497. 032435	−75.3 (−18.00)	178.17	
TS2s	−497.011651	−20.8 (−4.96)	102.48	i2269.7
PN-2Q3J4Q	−497.038474	−91.2 (−21.79)	110.50	
TS2s-0	−497.017370	−35.8 (−8.55)	105.21	
TS2s-1	−497.013852	−26.5 (−6.34)	108.93	i504.1
PN-2Q3* + HO_2	−497.027984	−63.7 (−15.21)	147.00	
TS2s-2	−497.021226	−45.8 (−10.97)	110.92	
2Q-3,4CY + OH[c]	−497.067018	−166.1 (−39.71)	137.77	
vdW BIR-OH[d]	−497.004916	−3.1 (−0.74)	111.65	
PN-2OJ4QJ(T) + OH	−496.987068	43.8 (10.46)	139.83	
PN-2OJ4QJ(S) + OH	−497.003303	1.17 (0.28)	137.35	
TS4 (OH expel)	−497.002646	2.9 (0.69)	101.27	i584.5
2,4-trioxane + OH	−497.021624	−46.9 (−11.22)	130.48	
TS5	−496.975231	74.8 (17.89)	108.17	i1913.3
keto-zQ + OH	−497.051191	−124.5 (−29.77)	137.47	
TS5-1	−497.035761	−84.1 (−20.09)	138.16	i281.3
DMC + CH_3CHO + OH[e]	−497.041517	99.2 (−23.70)	179.80	
TS-O-insertion + OH	−497.011890	21.4 (−5.11)	139.85	i851.2
perdioxetane + OH	−496.978573	66.1 (15.79)	130.10	
TS5-2A_H_2O_2 + OH[f]	−497.022262	49.5 (−11.85)	138.48	i387.6
PN-2*O4* + H_2O_2	−497.072119	179.5 (−42.91)	140.14	

[a] Relative to entrance channel enthalpies. [b] Imaginary modes for transition states. [c] 2Q-3,4CY represents the oxirane structure formed via TS2s-2 (Figure 2). [d] BIR represents singlet biradical PN-2OJ4QJ (see text). [e] DMC represents dimethyl Criegee intermediate (acetone oxide). [f] This pathway is not shown in Figure 9.

channel PN-2Q4J + O_2 = PN-2*O4OJ + 2OH is chain branching as it generates two OH and one alkoxy radical.

PN-2Q4J + O_2 = *PN-2Q4QJ* (well depth = 36.9 kcal mol^{-1})

PN-2Q3J4Q = *PN-2*O4Q* + *OH* (*TS-1s*, $\Delta H^{\#}$ = 15.7 kcal mol^{-1})

*PN-2*O4Q* = *PN-2*O4OJ* + *OH* (BDE = 47.9 kcal mol^{-1})

PN-2Q4J + O_2 = *PN-2*O4OJ* + *2OH*

(B) Biradical Channel. The second important chain branching path is the formation of a singlet biradical (and its van der Waals complex with the leaving OH group H-bonded to peroxy oxygen as illustrated in Figure 3).

net: PN-2Q4J + O_2 → PN-2Q4QJ* →

singlet-PN-2OJ4QJ + OH $\Delta H_{rxn} = -9$ kcal mol^{-1}

As seen from Figure 2, cleavage of the RO−OH (hydroperoxide) bond in the energized hydroperoxide peroxy radical (PN-2Q4QJ) that was formed by H-atom transfer prior to the second oxygen association faces a barrier of 36.2 kcal mol^{-1}, this is 0.7 kcal mol^{-1} below the entrance channel. This reaction leads to the formation of a biradical, 2-oxy-4-peroxy, PN-2OJ4QJ + OH. The dissociation energy incorporates a stabilization via formation of an intermolecular complex in the product set, Figure 3. Overall this new biradical path has a reaction barrier below the entrance channel and is chain branching. The reaction is expected to occur via both chemical activation and dissociation of the stabilized adduct at low to intermediate temperatures in combustion environments due to the high pre-exponential factor of the simple dissociation step.

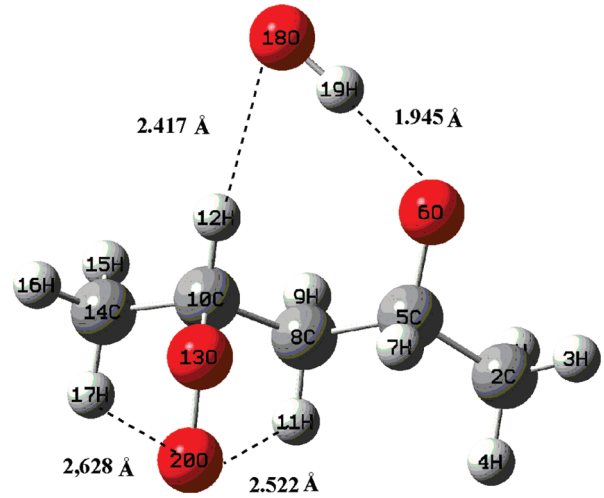

Figure 3. VdW Complex between the singlet *anti*-PN-2OJ4QJ biradical and leaving OH group.

The higher-spin triplet biradical intermediate is localized at 8.17 kcal mol^{-1} above the entrance channel; the energy of 45.1 kcal mol^{-1} to this product is in full agreement with the commonly accepted RO−OH bond dissociation energy for the second O_2 adduct in previous studies on smaller HC molecule systems.[1]

PN-2Q4QJ = triplet-PN-2OJ4QJ + OH

The bond dissociation enthalpy on the triplet surface is calculated to be 45.1 kcal mol^{-1}, while decomposition on the singlet surface, as indicated above, is lower, with BDE = 36.2 kcal mol^{-1}.

The 2-oxy-4-peroxypentane biradical PN-2OJ4QJ may further decompose to acetaldehyde and a smaller 1-oxy-2-propane biradical, $CH_2JC(OOJ)CH_3$.

$$PN\text{-}2OJ4QJ(+OH) = CH_3CHO + CH_2JC(OOJ)CH_3(+OH)$$

We note that the fate of the biradical PN-2OJ4QJ, either triplet or singlet, is not apparent. The triplet biradical can decompose through a number of paths, some of which are complex and currently under study in our group. These include the following:

(i) The spin-forbidden reaction to triplet oxygen, acetaldehyde, and propene

$$PN\text{-}2OJ4QJ = {}^3O_2 + CH_3CHO + CH_2CHCH_3$$
$$\Delta H_{rxn} = -9.5 \text{ kcal mol}^{-1}$$

The release of a triplet oxygen can also be accompanied by a ring closure at the 2,4-positions (via the alkoxy oxygen attack on the C(4) atom bearing the peroxy group by forming 1,3-dimethyloxetane)

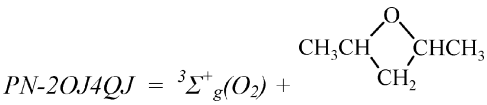

(ii) Decomposition into a formaldehyde and two acetaldehyde molecules

$$PN\text{-}2OJ4QJ = 2CH_3CHO + CH_2O$$
$$\Delta H_{rxn} = -86 \text{ kcal mol}^{-1}$$

This process occurs as the first CH_3CHO is leaving the peroxy oxygen bonds to the new radical, forming a dioxetane with sufficient energy to cleave the peroxide bond. While this is not a direct chain branching, it is a highly energetic reaction.

(iii) Elimination of CH_3 (β-scission) with the formation of a butan-1-al-4-peroxy radical

$$PN\text{-}2OJ4QJ = CH_3 + CHOCH_2CH(OOJ)CH_3$$

This pathway has a 22 kcal mol^{-1} activation energy to the lowest-energy conformer of the formed peroxy radical.

Chain branching in this PN-2Q4J + O_2 system through the formation of a biradical is more apparent if one considers the energetically more preferred singlet biradical (the reaction energy is lower by ~8 kcal mol^{-1} than the triplet, vide supra). A spin-allowed reaction path involves dissociative ring closure with the generation of a reactive singlet oxygen molecule $^1\Delta_g(O_2)$ accompanied only by the 7.49 kcal mol^{-1} energy gain.

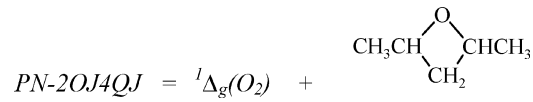

In biochemical media, singlet oxygen $^1\Delta_g(O_2)$ is a well-known source for peroxidation of biomolecules, particularly lipids,[28] and the generation of a reactive singlet oxygen could provide chain branching features in conjunction with the OH radical that is also released. The role of singlet oxygen in combustion media is still uncertain, and there is limited literature data on this important reaction process (there is some discussion in (ref 5b).

Further study of these diradical reactions in the above system is in progress.

(C) Oxirane Channel. The energized [PN-2Q4QJ]* and stabilized PN-2Q4QJ adducts can undergo reaction to a dihydroperoxide alkyl radical, PN-2Q3J4Q, via intramolecular 1,4-H-atom transfer. This radical can then undergo a ring closure transition state to form an oxirane plus OH via TS2s-2, which is 10.4 kcal mol^{-1} below the entrance channel; it subsequently leads to the elimination of an OH radical and formation of an oxirane hydroperoxide intermediate (denoted in Table 2 as PN2Q-3,4CY). The oxirane hydroperoxide can further decompose and release another OH radical along with the acetaldehyde and methyloxiranyl cyclic carbon radical (the methyloxiranyl radical). The overall process is also chain branching.

We discuss this sequence of reactions in more detail below.

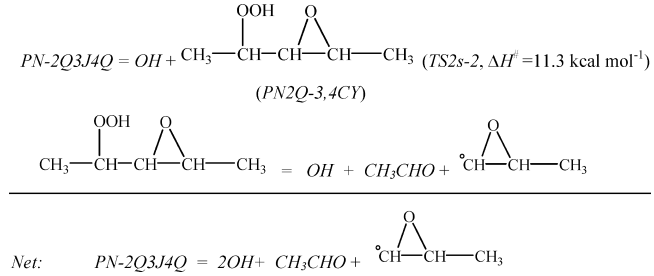

(D) HO_2 Elimination Channels. There are two paths to form an olefin hydroperoxide plus HO_2 radical.

(i) The dihydroperoxide alkyl (carbon) radical, PN-2Q3J4Q intermediate, can eliminate (β-scission) a hydroperoxy radical via the TS2s-1 transition state

$$PN\text{-}2Q3J4Q = PN\text{-}2Q3^* + HO_2$$
$$(\text{TS2s-1}, \Delta H^{\#} = 15.5 \text{ kcal mol}^{-1})$$

(ii) A second path is a molecular elimination from the PN-2Q4QJ adduct over transition state TS2s-0 (28.4 kcal mol^{-1}). This transition state leads to the same HO_2 + PN-2Q3* product set and is 6.3 kcal mol^{-1} below the entrance channel, as illustrated in Figure 2 and detailed in Table 2. As noted above, this elimination of HO_2 eventually results in chain termination at temperatures below 900 K, at which these peroxy reactions occur, through the formation of H_2O_2.

(E) Pathway Comparison of HC Radical Oxidation: Second O_2 (TS-s) versus First O_2 (TS-f). The well depth in the second oxygenation stage is slightly decreased, 36.9 versus 37.5 kcal mol^{-1} for the first peroxy radical formation. Several comparative values on 1,4- and 1,5-hydrogen transfer reaction barriers are collected in Table 3.

The barrier for concerted HO_2 elimination from the peroxy adduct, formation of olefin plus HO_2, is reduced for the second oxygen system to 28.4 relative to 30.1 kcal mol^{-1} in PN-2QJ.

Reactions to and from the α*-H-Atom Transfer Reaction (1,4-H Shift).* Barriers for α-hydrogen (1,4)-transfer (via a five-member ring) from a secondary alkyl carbon to the peroxy radical oxygen are slightly increased in the hydroperoxide peroxy system (second stage) where transition states TS2f and TS2s are 31.3

TABLE 3: Comparative Analysis of 1,4(α)- and 1,5(β)-H-Transfer Paths[a]

	TS (step 1)	$\Delta H^{\#}$	TS (step 2)	$\Delta H^{\#}$
HO_2 direct	2f-0	30.1	2s-0	28.4
α-H-transfer	2f	31.3	2s	32.0
HO_2 formation	2f-1	14.8 (29.6)[b]	2s-1	15.5 (30.7)
oxirane formation	2f-2	9.1 (23.9)[b]	2s-2	11.3 (26.5)
β-H-transfer	1f	19.7	1s	15.7
oxetane formation	1f-1	16.1	n/a	branching
decomposition	1f-2	24.9 (38.7)		

[a] Units: kcal mol^{-1}. [b] Values relative to the adducts' barrier heights are in parentheses.

versus 32.0 kcal mol^{-1}, respectively. The barriers for subsequent HO_2 elimination from the alkyl radical (βsc to form an olefin plus HO_2) is increased slightly in the second O_2 association at 14.8 and 15.5 kcal mol^{-1}, respectively.

The oxirane formation pathway in the hydroperoxide alkyl radical is more favorable in the first O_2 association system with barriers of 9.1 versus 11.3 kcal mol^{-1} in the dihydroperoxide alkyl radical.

Reaction to and from the β-H-Atom Transfer Reaction (1,5-H Shift). Barriers for β-hydrogen (1,4)-transfer (five-member ring) from a secondary alkyl carbon to the peroxy radical oxygen are slightly increased in the hydroperoxide peroxy system (second stage) where transition states TS1f and TS1s are low (19.7 and 15.7 kcal mol^{-1}, respectively).

The oxetane formation pathway in the dihydroperoxide alkyl radical would involve formation of a primary alkyl radical and should not be compared with the value 7.7 kcal mol^{-1} for the monohydroperoxide system that involves a secondary alkyl radical.

3.3. Summary of Chain Branching Reaction Schemes. (a) The main chain branching channel in this series of two O_2 association (chemical activation) reactions is

$$\text{PN-2Q4J} + O_2 = \text{PN-2Q4QJ} \qquad (\text{well depth} = 36.9 \text{ kcal mol}^{-1})$$

$$\text{PN-2Q3J4Q} = \text{PN-2*O4Q} + \text{OH} \qquad (\text{TS-1s}; \Delta H^{\#} = 15.7 \text{ kcal mol}^{-1}, \Delta H_{rxn} \text{ from R} + O_2 = -65.9 \text{ kcal mol}^{-1})$$

$$\text{PN-2*O4Q(+OH)} = \text{PN-2*O4OJ} + \text{OH(+OH)} \qquad (\text{BDE} = 47.9 \text{ kcal mol}^{-1})$$

(b) The second chain branching path includes formation of a singlet oxypentylperoxy biradical PN-2OJ4QJ, which further decomposes via several pathways.

$$\text{PN-2Q4QJ} = \text{PN-2OJ4QJ} + \text{OH} \qquad (\text{BDE} = 36.2 \text{ kcal mol}^{-1})$$

TABLE 4: Comparison of Well Depth and Barriers[a]

	well depth	H-shift five-member ring	HO_2 elimination	H-shift six-member ring
ethyl[b]	35.0	36.0 primary	30.5	
sec-propyl[c]	37.5	36.0 primary	30.0	
n-propyl[c]	35.9	32.0 secondary	30.0	23.0 primary
sec-pentyl[d]	37.0	31.0 secondary	30.1	19.0 secondary

[a] Units: kcal mol^{-1}. [b] Reference 1b. [c] Reference 24. [d] Secondary pentyl as a representative for larger hydrocarbon radicals features five- and six-member ring H-transfer reactions from a secondary C position to the peroxy centers.

$$\text{PN-2OJ4QJ(+OH)} = CH_3CHO + CH_2JC(OOJ)CH_3\text{(+OH)}$$

$$\text{PN-2OJ4QJ} = {}^3O_2 + CH_3CHO + CH_2CHCH_3$$

$$\text{PN-2OJ4QJ} = 2CH_3CHO + CH_2O$$

PN-2OJ4QJ = $^3\Sigma^+_g(O_2)$ + 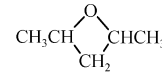 (1,3-*Dimethyl-Oxetane*)

$$\text{PN-2OJ4QJ} = CH_3 + CHOCH_2CH(OOJ)CH_3$$

PN-2OJ4QJ = $^1\Delta_g(O_2)$ + 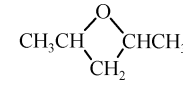

(c) The adduct PN-2Q4QJ can undergo intramolecular 1,4-H (five-member ring) transfer to intermediate PN-2Q3J4Q dihydroperoxyalkyl radical, which further decomposes in two steps by releasing a hydroxyl radical in each step. In conjunction with the first hydroxyl radicals released upon ring closure in PN-2Q3J4Q to oxirane hydroperoxide (denoted in Table 2 as 2Q-3,4CY), this channel can lead to the chain branching.

$$\text{PN-2Q3J4Q} = \text{PN2Q-3,4CY} + \text{OH} \qquad (\text{TS2s-2}, \Delta H^{\#} = 11.3 \text{kcal mol}^{-1})$$

PN2Q-3,4CY =OH + CH3CHO+ 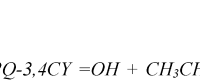 (*Methyl-Oxiranyl radical*)

ΔH =58.5 kcal mol^{-1}

3.4. Some Comparison with the Simpler Homologues. Relative barrier values for ethyl radical + O_2 and primary and secondary propyl radical + O_2 along with the corresponding data for the secondary pentyl radical + O_2 system[1b,d,24] are presented in Table 4. In general, the data are consistent and lend support for the accuracy of our calculation. The well depth increases slightly (deeper wells) for secondary sites as the size of the radical increases. The secondary propyl has a slightly (0.5 kcal mol^{-1}) deeper well depth than the 2-pentyl radical + O_2. We note that the barrier for direct HO_2 elimination remains almost unchanged in all of the systems (see Tables 3 and 4).

4. (Kinetic) QRRK Master Equation Analysis

Chemical activation and unimolecular dissociation kinetic analysis is performed on the reaction systems illustrated in the enthalpy diagrams (Figures 1 and 2); enthalpies are scaled to the

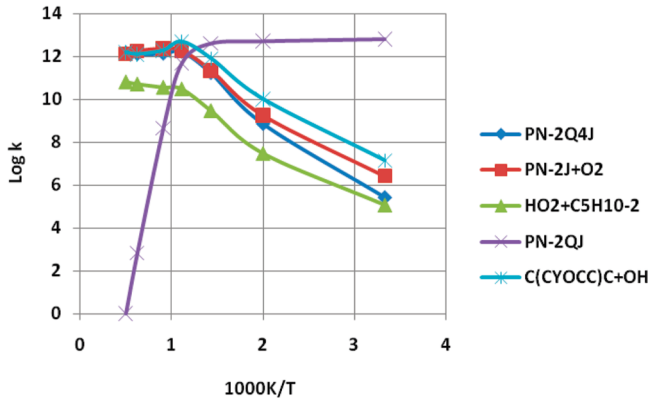

Figure 4. Rate constants of first chemical activation reactions (PN-2J + O_2) as a function of temperature at 1 atm pressure. C(CYOCC)C stands for the 1,3-dimethyloxetane (see text).

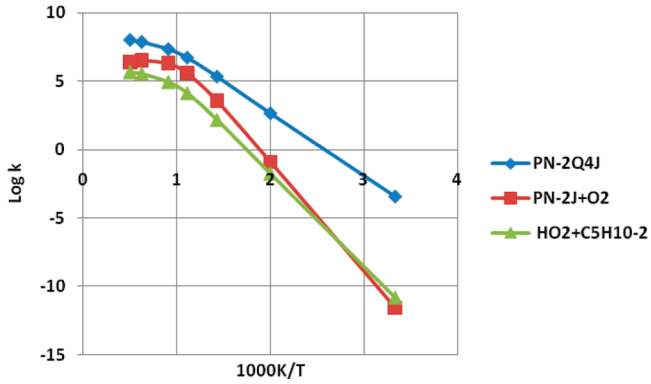

Figure 5. Temperature dependence of dissociation rate constants for the PN-2QJ adduct at $P = 1$ atm. C(CYOCC)C stands for the 1,3-dimethyloxetane (see text); log k versus 1000/T.

$\Delta H_f°_{298}$ of PN-2J + O_2 and PN-2Q4J + O_2 reactants set to zero. The association potential curve with O_2 was analyzed with B3LYP, BMK, and TPSSLYP1W DFT methods, in conjunction with the 6-31G(d,p) and 6-311+G(2d,p) basis sets. High-pressure-limit rate constants and transport parameters for the two reaction systems are listed in Appendix 2 Table A2. Kinetic results are based on the association rate constants using a VTST analysis that neglects hydrogen bond formation features along association paths (see Appendix 3).[1c,20]

Reaction kinetic parameters for the formation of energized alkylperoxy and hydroperoxide alkylperoxy adducts, their reactions to stabilization, and new product formation as well as their reverse channels were determined using multifrequency QRRK analysis for $k(E)$[1,27] with the steady-state assumption on the energized adduct(s) and master equation (ME) analysis for falloff. A $(\Delta E)°_{down}$ of 830 cal mol^{-1} was employed in the ME analysis with N_2 as a third body.

4.1. First O_2 Addition Channels. The chemical activation rate constants and branching ratios as function of 1000/T(K) at 1 atm pressure for the PN-2J + O_2 chemical activation and the dissociation reactions of the stabilized PN-2QJ peroxy radical are illustrated in Figures 4 and 5 and detailed below.

(A) PN-2J + O_2 Chemical Activation Reaction. The chemical activation reaction of the PN-2J + O_2 (Figure 4) shows that stabilization of the peroxy radical PN-2QJ is the dominant channel up to near 1000 K, where formation of the stabilized hydroperoxide alkyl PN-2Q4J adduct increases steadily with temperature. At 1000 K, it is formed at similar rates to the peroxy radical, which is now in the falloff.

The PN-2Q4J, which can undergo chain branching reaction. The oxirane + OH and the chain termination 2-pentene plus HO_2 steps are approximately one and two orders of magnitude below the PN-2Q4J formation to well above 1000 K.

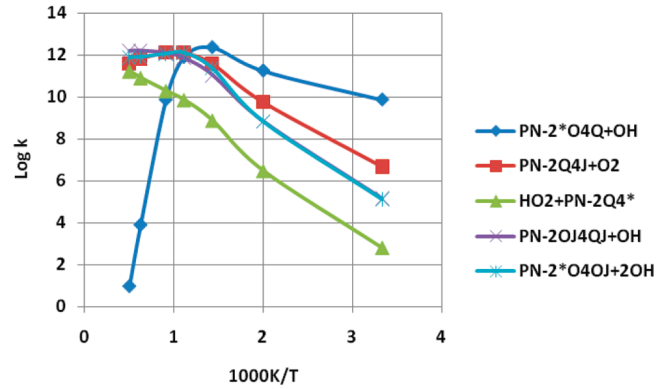

Figure 6. Rate constants of second chemical activation reactions (PN-2Q4J + O_2) as a function of temperature at 1 atm pressure.

(B) PN-2Q4J Dissociation Reactions. Dissociation of the stabilized PN-2QJ shows the same trend as that seen in the chemical activation steps (see Figure 4). The PN-2Q4J isomer dominates the oxirane plus hydroxyl and HO_2 molecular elimination channels to temperatures above 1000 K.

4.2. Second O_2 Addition Channels. Calculated reaction paths for this more complex reaction system are illustrated in the potential energy diagram presented in Figure 2. Several of the above-noted nonconventional reaction paths, which have higher barriers (near or above the entrance channel) in this second O_2 association system, are omitted in the QRRK/ME calculations and will be analyzed in a future study.

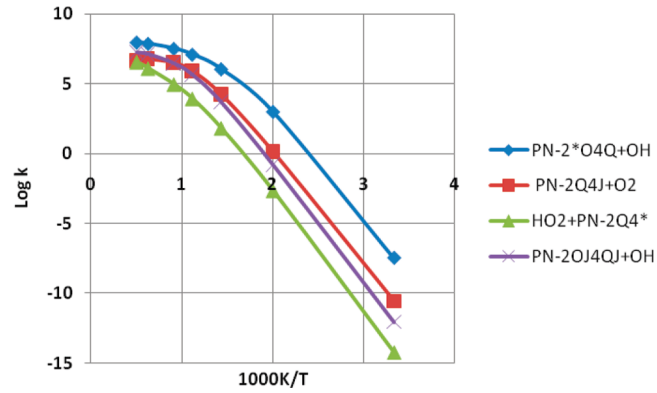

Figure 7. Temperature dependence of dissociation rate constants for the PN-2Q4QJ adduct at $P = 1$ atm.

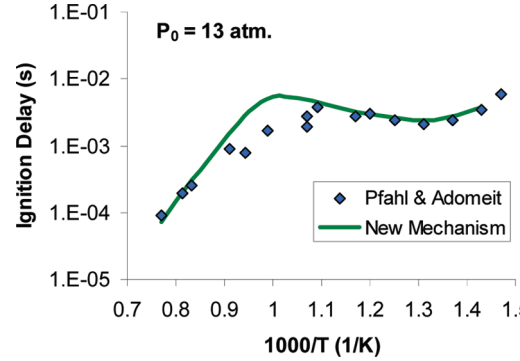

Figure 8. Ignition delay times of an *n*-decane−air mixture (N_2 bath gas) versus the inverse of the initial temperature. The mechanism denoted as "New Mechanism" involves the main modifications described above for *n*-pentane and modified for *n*-decane. Note that the mechanism is not adjusted to get more consistency with experimental values of ref 28 at temperatures of 1000−1200 K, where deviations might be predetermined by the governing role of the other reactions (such as decomposition of H_2O_2).

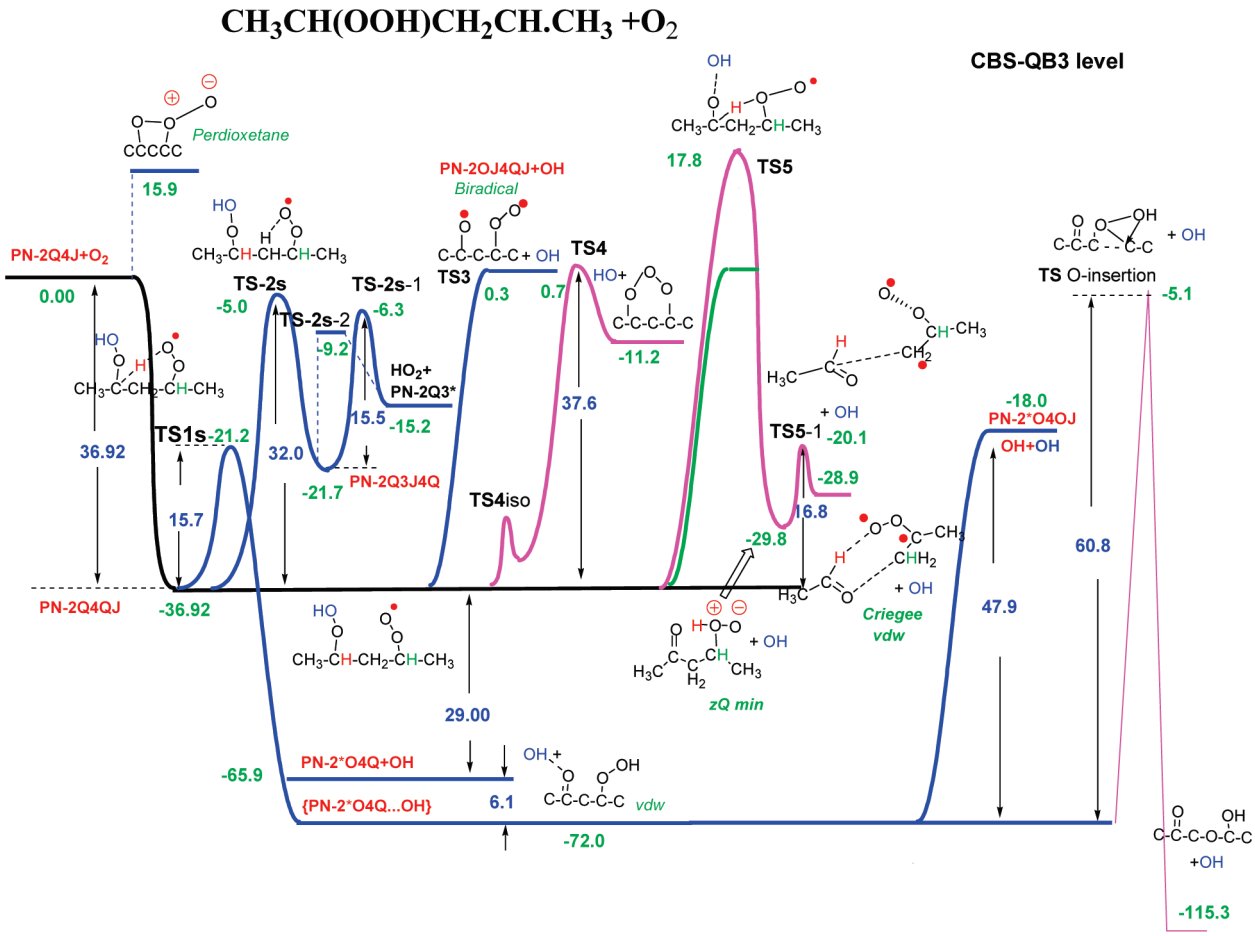

Figure 9. Detailed enthalpy diagram for the second chemical activation reaction, addition of oxygen to the 2-hydroperoxy-4-*n*-pentyl radical (PN-2Q4J + O_2), calculated at the CBS-QB3 level. There are some other mechanisms, more sophisticated and somewhat higher in energy, which are omitted for the sake of clarity.

(A) PN-2Q4J + O_2 Chemical Activation Reactions. Figure 6 illustrates the rate constants for the chemical activation reaction of the PN-2Q4J + O_2 reaction system at 1 atm versus 1000/*T*. The stabilized hydroperoxide peroxy radical PN-2Q4QJ is the main product up to 900 K. The ketohydroperoxide plus OH radical formation (PN-2*O4Q + OH) and the chain branching 2-pentanone-4-oxy radical + 2OH reactions become competitive at 600 and 900 K, respectively. The biradical (PN-2OJ4OJ) + OH channel mirrors the 2-pentanone + 2OH reaction path. The stabilized hydroperoxide peroxy radical, the ketohydroperoxide + OH, and the two chain branching reactions (2-pentanone-4-oxy + 2 OH and biradical + OH) are the dominant reaction processes in this reaction system.

Dissociation of [PN-2*O4Q]* versus stabilization is calculated using the fraction of energy from the H-transfer barrier remaining in this carbonyl intermediate based on its reduced number of vibrations after loss of OH (Figure 6). The energy allocation from the entrance channel to the [PN-2*O4Q]* + OH products is 72 kcal mol^{-1}; this is more than sufficient at combustion conditions to result in simple cleavage in the remaining RCO−OH peroxide bond prior to stabilization.

(B) Unimolecular Dissociation Reactions of the Stabilized PN-2Q4QJ Adduct. Rate constants for dissociation of the PN-2Q4QJ (2-hydroperoxide-4 peroxy pentane) radical versus 1000/*T* at 1 atm are illustrated in Figure 7. The dominant path at low temperatures is the ketohydroperoxide plus OH (PN-2*O4Q + OH) reaction path. At 850 K and above, the two chain branching paths 2-pentanone-4-oxy + 2OH and biradical PN-2OJ4OJ + OH become the dominant forward reaction paths with near identical rate constants. The reverse reaction, back to the PN-2Q4QJ peroxy radical has kinetics that are similar to the two chain branching paths.

(C) Unimolecular Dissociation Reaction of the Stabilized PN-2*O4Q adduct. The lowest barrier for reaction of the 2-keto-4-peroxy radical, PN-2*O4Q, is unimolecular dissociation, cleavage of the weak RO−OH peroxy bond, where we calculate the bond energy as 47.9 kcal mol^{-1}. This dissociation will form an alkoxy radical + OH, where the alkoxy radical will undergo βsc reactions

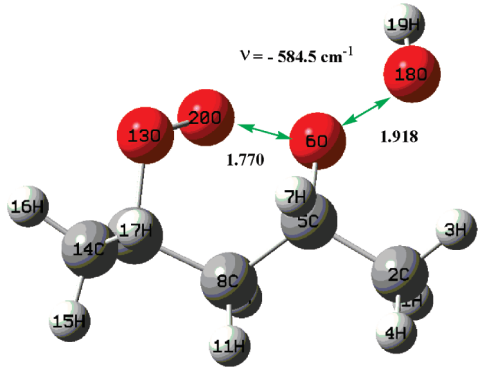

Figure 10. Transition state TS4 for the intramolecular expel of the OH group in chemically activated adduct PN-2QJ4Q. The terminal O(20) atom of the peroxy group attacks the O(6) internal (proximal) atom of the hydroperoxy group, yielding semiozonid 1,2,3-trioxane structure and a OH radical.

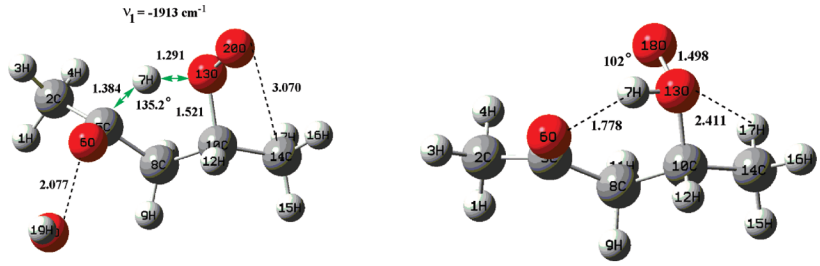

Figure 11. (a) Transition state TS5 of zwitterionic keto-zQ intermediate formation from peroxy hydroperoxide, adduct PN-2Q4QJ. H(7) transfers to the proximal O(13) while the O(18)−H(19) group is leaving; see Figure 9. TS is stabilized by a vdW complex between a biradical and the leaving OH group. (b) Optimized at the CBS-QB3 level keto-zQ zwitterionic structure, consistent with the results of QCISD/6-31G(d,p), MP2/6-311G(2df,p), and B3LYP/6-311G(2df,p) individual and G3MP2 composite-level predictions.

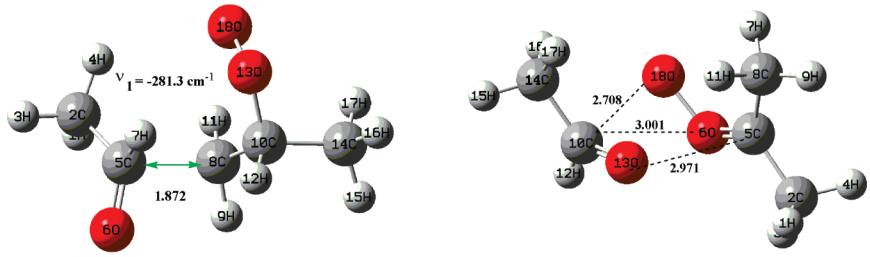

Figure 12. (a) Transition state TS5-1 of the skeletal C(5)−C(8) bond fission reaction resulting in the formation of acetone oxide; the H(7) atom of the keto-zQ structure is spontaneously shifted to the C(5) atom of the carbonyl group. (b) A 1,2-H shift from central C(10) atom of the peroxy fragment to the newly formed terminal carbon radical center C(8) forms the product set acetone oxide (dimethyl Criegee intermediate) and acetaldehyde, which are additionally stabilized in a vdW complex.

to (i) acetaldehyde plus an acetone radical, (ii) methyl radical plus 2-keto butanal, or (iii) pentane-2,4-dione plus H atom.

(D) QRRK Output Kinetic Data. Selected kinetic data output from the chemical activation reaction analysis and the corresponding dissociation reactions of stabilized adducts are located in Appendix 4 Table A3. More extended data are listed in the electronic Supporting Information.

4.3. Mechanism Modeling with the dual Oxygen Association Reaction Sequence. The above kinetic scheme, which incorporates pressure- and temperature-dependent dissociation and chemical activation reactions, has been incorporated in our detailed *n*-Decane kinetic model[29] with pressure and temperature corrections to the rate constants for *n*-decane. As seen in Figure 8, predicted ignition delay times versus temperature show very good agreement with observed data[28] at low temperature as well as high temperatures.

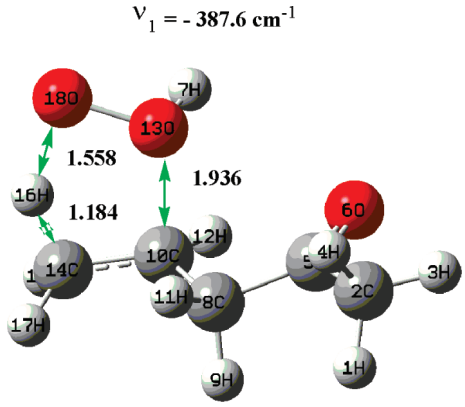

Figure 13. Keto-zQ converts to the H_2O_2 + PN-1*4O via transition state TS5-2 (cf. Figure 2b).

At intermediate temperatures, agreement is poorer. We emphasize that the mechanism has not been adjusted to obtain more consistency with experimental values[28] at temperatures 1000−1200 K where deviations might be predetermined by the governing role of the other reactions (such as decomposition of H_2O_2). More complete account of this mechanism and its validation can be found in ref 29. We note that there are many detailed reaction mechanisms for normal hydrocarbon oxidation that model the negative temperature dependence observed in experiments. To our knowledge, this is the only mechanism for normal hydrocarbons with secondary carbon radicals that has temperature and pressure analysis for chemical activation and unimolecular dissociation reactions of the peroxy species.

5. Nontraditional Channels in the PN-2Q4J + O_2 Second Oxygenation Reaction

The larger size of common fuel molecules relative to the smaller homologues, where reaction kinetic parameters and thermochemistry are often analyzed in detail, motivates an analysis for possible new chemical transformation channels in these larger molecules. On the PES for PN-2Q4J + O_2, we have identified several new pathways affected by the larger carbon chain; they are presented in Figure 9. Pathways already considered in section 3.2 are included for completeness (cf. also Table 2). Several of these novel channels are considered plausible, and they may be relevant in the more complex reaction paths that occur in the combustion of large hydrocarbons, real fuel systems.

(A) Trioxane Formation. A new relatively low energy (on the level of entrance channel) dissociative ring closure reaction of the peroxy center to form a semiozonid structure (1,2,3-trioxane) is identified from reaction of the PN-2Q4QJ peroxy adduct. The reaction occurs via peroxy radical attack on the oxygen bonded to the carbon of the hydroperoxide with elimination of the OH group. TS4 in Figure 10 illustrates the unique structure of the transition state leading to the

formation of the trioxane structure. This might be considered similar to alkyl radical attack on the peroxide group, which results in the well-established formation of cyclic ethers, albeit more complex electronically, and formation of a weaker bond. The barrier to the reaction from the PN-2Q4QJ peroxy radical is only 37.6 kcal mol^{-1}.

The research groups of Nick Cernansky and Dave Miller have recently quantified appreciable levels of trioxane formation in their moderate-temperature oxidation experiments on *n*-dodecane using a pressurized flow reactor apparatus updated with a direct injection GC/MS inlet.[30] They interpreted the trioxane formation as a result of formaldehyde polymerization and consequently associated it with a symmetric 1,3,5-trioxane structure. We note that polymerization of formaldehyde usually occurs at lower temperatures than those found in their oxidation experiments and that the mass spectrometric method used by authors may not have been able to differentiate the specific isomer of trioxane. It is possible that their detected compound might be the asymmetric 1,2,3-isomer of trioxane, which we described in the formation mechanism above. Further clarification of their structure could be of value in support of our calculated pathway.

(B) Zwitterion Formation. Formation of a zwitterionic keto-hydroperoxide intermediate (keto-zQ, Figure 9) is a nonconventional 1,4-H-transfer reaction from the carbon atom of the hydroperoxide group in the PN-2Q4QJ adduct (2-hydroperoxide-4-pentylperoxy radical) to the oxygen bonded to the carbon of the peroxy radical group via transition state TS5 (see Figure 11). This transition structure represents a concerted OH elimination/hydrogen transfer in the PN-2Q4QJ adduct to form a zwitterionic ketone and new hydroperoxide moiety. To the best of our knowledge, the reaction path is new and unique. The transition state of the 1,4-H-transfer reaction is stabilized (reduced) via a van der Waals (vdW) complex with the leaving OH group. The resulting TS5 barrier is 17.8 kcal mol^{-1} higher than the PN-2Q4J + O_2 entrance channel. However, this barrier is stabilized by ~3 kcal mol^{-1} (lower) relative to the alternative stepwise mechanism via the preliminary formation of the biradical path (green line in Figure 8) and the further H transfer from C(2) to the corresponding central O atom attached to the C(4) atom to form the keto-zQ zwitterionic ketohydroperoxide intermediate. We shall discuss the stability and plausible reaction kinetics (e.g., high-temperature or singlet $^1\Delta_g$ O_2 reaction systems) for this keto-zQ system in future work.

We propose that this mechanism may occur under combustion conditions. For example, it could occur in a reaction of a hydroperoxide alkyl radical with singlet oxygen $^1\Delta_g(O_2)$ with the added 22.5 kcal mol^{-1} in chemical activation relative to ground-state triplet oxygen $^3\Sigma_g^+(O_2)$. One might consider that this reaction might occur in presence of singlet oxygen reaction with hydroperoxide alkyl radicals in biological media and possibly in atmospheric chemistry. Singlet oxygen is known to be formed in the troposphere by ozone photolysis.

The structure of keto-*zQ* (Figure 11b) calculated at the CBS-QB3 level is confirmed by the higher-level ab initio QCISD/6-31G(d,p) as well as MP2/6-311G(2df,p) and B3LYP/6-311G(2df,p) individual and G3MP2 composite-level calculations with full optimization of all internal variables. Nevertheless, additional MCSCF analysis would help to verify single-reference character of this intermediate. Biradical/zwitterionic structures are commonly accepted as intermediates in reactions of singlet oxygen $^1\Delta_g(O_2)$ with unsaturated organic molecules, where these reactions are often studied within the CASSCF//CASPT perturbative calculation methods.[31]

Two further reactions of this *keto*-zQ intermediate are identified, (i) an endothermic transformation with a barrier of only 8.8 kcal mol^{-1} involving a double H-transfer process to form the $(CH_3)_2C^{\bullet}OO^{\bullet}$, the dimethyl derivative of the Criegee intermediate (CH_2OO), and the acetone oxide (Figure 12) and (ii) The keto-zQ intermediate, which can also undergo exothermic H_2O_2 elimination reaction via TS5-2A; see the structure in Figure 13 and Table 2 (the pathway is not shown in Figure 9), where the barrier height is calculated as 18 kcal mol^{-1}.

$$\text{keto-zQ} = H_2O_2 + \text{PN-1*4O} \qquad (\Delta H^{\#} = 18 \text{ kcal mol}^{-1}, \Delta H_{rxn} = 13.1 \text{ kcal mol}^{-1})$$

This pathway can be considered as a new relevant hydrogen peroxide formation channel for HC combustion at low temperatures.

(C) Other Relevant Channels. There are several other intramolecular transformation channels for the PN-2*O4Q ketohydroperoxide structure formed in the PN-2Q4J + O_2 activation step. One interesting channel is the exothermic insertion reaction of an O atom from the peroxy group into the carbon backbone illustrated in Figure 9 and denoted as TS O insertion. While the barrier for this reaction is significant relative to the stabilized PN-2*O4Q, it is still lower than the entrance channel for the peroxy radical formation. This is a result of the large exothermicity for formation of the carbonyl bond (via TS1s). This oxygen insertion destroys the carbon backbone and may be accessed by the chemically activated product under combustion conditions.

Perdioxetane is another zwitterion structure localized 15.9 kcal mol^{-1} above the entrance channel (see Figure 9). It can be formed directly upon interaction of the PN-2Q4J radical with O_2, but due to the specific electronic structure of this compound, this pathway needs further clarification.

6. Conclusions

Quantum chemical DFT and CBS-QB3 calculations were performed on *n*-pentane as a surrogate for the higher molecular *n*-alkane oxidation because the peroxy radical formed at the secondary carbon radical site can undergo low-energy (19.7 kcal mol^{-1}) intramolecular hydrogen-atom transfer, resulting in a new alkyl radical site for O_2 association and chain branching. Several low-temperature chain branching and termination pathways are revealed, and stationary points are determined for the consecutive addition of two oxygen molecules to the 2-pentyl radical. Kinetic analysis shows the major paths of the second chemical activation association of the 2-hydroperoxide pentan-4-yl (PN-2Q4J) radical with O_2 are chain branching. The formation of the PN-2Q4J like radicals and their concentrations in combustion systems is important to the overall oxidation rate of normal alkanes. As seen from Figure 5, the PN-2Q4J is formed with considerable rates (cf. corresponding barrier on Figure 1). However, the reverse isomerization process, the reaction of PN-2Q4J back to the PN-2QJ peroxy radical, as demonstrated in Figure 1, has a low barrier (only 5.9 kcal mol^{-1}). The major reaction path for the dissociation reaction of the PN-2QJ peroxy radical is dissociation back to the 2-pentyl radical + O_2, where the entropic component of the free energy increases the importance of this reaction at higher temperature. The results of the individual DFT calculations, in general, are consistent with the relative energy features (sequences) predicted by the multilevel CBS-QB3 method. H-transfer barriers at the DFT level are ~2−3 kcal mol^{-1} higher than the higher-level CBS-QB3 results, in full accordance with the literature data for similar systems discussed in the Introduction.

Acknowledgment. The research was supported by the U.S. Air Force (Phase-II STTR Contract FA8650-06-C-2658). We thank Dr. Chris Montgomery of Reaction Engineering Design for evaluation of the *n*-decane mechanism (Figure 8). We are grateful to Dr. Craig Taatjes for providing a manuscript prior to publication (ref 21). Extremely detailed and valuable consideration of the manuscript by one of reviewers is also highly appreciated.

Appendix 1

Naming codes and corresponding schematic structures of main species are presented in Table A1.

TABLE A1: Naming Codes and Corresponding Schematic Structures for Main Species

Code	Structure (Formula)	Code	Structure (Formula)
PN-2J	C-C-C-C-C	PN-2*O4OJ keto-oxy	C-C-C-C-C
PN-2QJ	C-C-C-C-C	PN-2*O4Q	C-C-C-C-C
PN-2Q3J	C-C-C-C-C	2,4-Trioxane	C-C-C-C-C
PN-2Q4J	C-C-C-C-C	PN-2*O4HQJ (Keto-zQ)	C—C-C-C—C
PN-2Q4QJ	C-C-C-C-C	DMC	CH_2-C-CH_3
PN-2*O4Q (Keto-Q)	C-C-C-C-C	Perdioxetane	C-C-C-C-C
PN-2Q3J4Q	C-C-C-C-C	PN-2*O4*	C-C-C-C=C
PN-2Q3*	C-C-C=C-C	2Q-3,4CY	C-C-C-C
2Q-3,4CY	C-C-C-C-C		
PN-2OJ4QJ (BIR)	C-C-C-C-C		

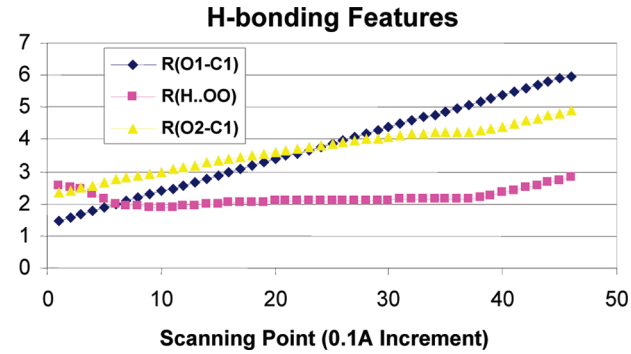

Figure 15. Competitive interactions of an attacking oxygen molecule with the radical center represented by the O1−C1distance (see the inset in Figure 14) and the terminal hydrogen atom represented by the H···OO distance versus the relative dissociation energy of primary Pr−O_2 (relaxed scanning results in Figure 14 above).

Appendix 2

H-Bonding Features in the Association of O_2 with the Hydrocarbon Radicals. While considering the entrance channel variational transition-state rate constant for the pentyl radical with oxygen, we noticed that hydrogen bonding along the association reaction pathway could play a significant role. We have performed detailed analysis of steric transformations along the association reaction pathway as this analysis is important for the kinetic analysis. Results for the secondary $C_3H_7 + O_2$ (PR-2J + O_2) association reaction are presented here. The results for PN-2J + O_2 are more complex and include additional deformation of the carbon backbone along the reaction path. The calculated dissociation curve for the isopropyl radical R−O_2 at the TPSSLYP1W density functional theory level is illustrated in Figure 14. The TPSSLYP1W functional is recommended as one of the best meta GGA DFT methods to reproduce H-bonding features, tested on $(H_2O)_n$ clusters.[32]

As seen from Figure 14, at R−O_2 distances of ~5 Å, the terminal (distal) O atom approaches the radical center while a

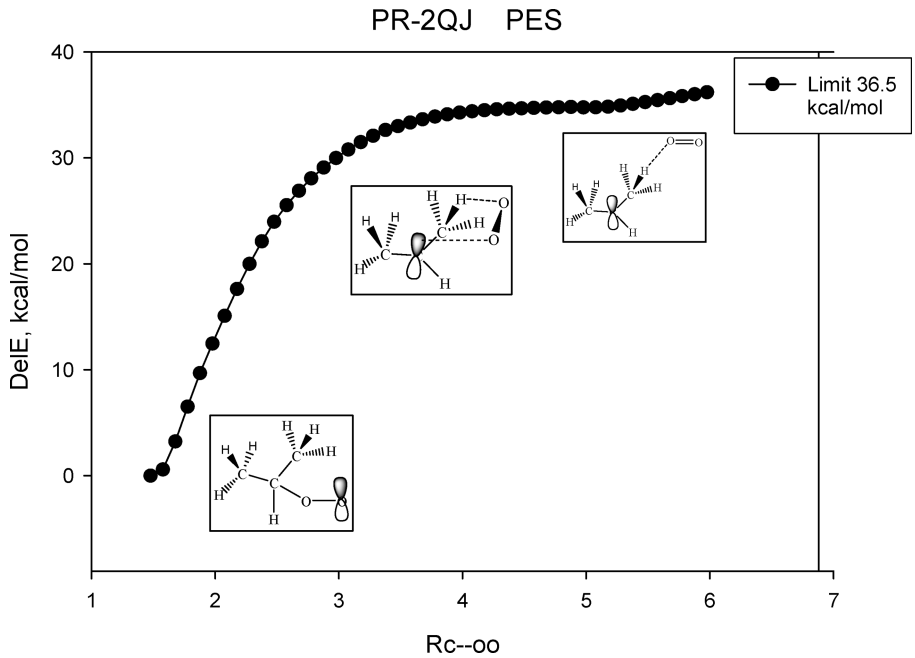

Figure 14. Potential energy profile of the dissociation reaction of the *sec*-propylperoxy radical as the *R*(C−OO) distance increases, calculated at the TPSSLYP1W/6-31G(d,p) level of theory.

TABLE A2: High-Pressure Rate Coefficients used in QRRK/ME Analysis (Modified Arrhenius Form)

	A	n	E_a
Reaction System PN-2J + O_2[a]			
PN-2J + O_2 → PN-2QJ	8.00×10^{13}	−0.44	0.0
PN-2QJ → PN-2J + O_2	2.46×10^{18}	−1.07	37.5
PN-2QJ → PN-2Q4J	9.00×10^{6}	1.59	19.7
PN-2QJ → HO_2 + C5H10-2	1.89×10^{7}	1.51	30.0
PN-2Q4J → PN-2QJ	4.80×10^{6}	0.91	5.9
PN-2Q4J → C(CYOCC)C + OH	2.04×10^{11}	0.0	16.0
Reaction System PN-2Q4J + O_2[b]			
PN-2Q4J + O_2 → PN-2Q4QJ	4.50×10^{13}	−0.44	0.0
PN-2Q4QJ → PN-2Q4J + O_2	8.2×10^{22}	−2.45	36.9
PN-2Q4QJ → PN-2*O4Q + OH	1.20×10^{10}	0.35	15.7
PN-2Q4QJ → HO_2 + PN-2Q4*	8.63×10	3.51	32.0
PN-2Q4QJ → PN-2OJ4QJ + OH	3.0×10^{15}	0.0	37.2
PN-2*O4Q + OH → PN-2Q4QJ	1.0×10^{8}	0.0	44.7
PN-2*O4Q + OH → PN-2*O4OJ + 2OH	3.0×10^{15}	0.0	

[a] Sigma (5.7 A), *e*/K (530 K), ΔE down (850 cal, no T dependence), integration interval (330 cal). [b] Sigma (5.9 A), *e*/K (630 K), ΔE down (850 cal, with no T dependence), integration interval (330 cal).

TABLE A3: Selected Rate Coefficients for Chemical Activation Reactions of PN-2J + O_2 (Dual Oxygenation of 2-Pentyl Radical) in Modified Arrhenius Form (P = 1 atm)

	A	n	E_a	
C_5H_{11}-2 + O_2 ⇔ PN-2QJ	6.66×10^{39}	−8.84	7095	!1.00E+00 (1.00E+00) atm, 300−1800 K, 16% err, 1.00 × N2
C_5H_{11}-2 + O_2 ⇔ HO_2 + C_5H_{10}-2	5.08×10^{19}	−2.43	11058	!1.00E+00 (1.00E+00) atm, 300−1800 K, 44% err, 1.00 × N2
C_5H_{11}-2 + O_2 ⇔ PN-2Q4J	3.63×10^{36}	−7.37	12745	!1.00E+00 (1.00E+00) atm, 300−1800 K, 54% err, 1.00 × N2
C_5H_{11}-2 + O_2 ⇔ C(CYOCC)C + OH	1.11×10^{28}	−4.53	16782	!1.00E+00 (1.00E+00) atm, 300−1800 K, 45% err, 1.00 × N2
Dissociation of Stabilized Adduct 1, PN-2QJ				
PN-2QJ ⇔ HO_2 + C_5H_{10}-2	2.85×10^{33}	−6.93	36484	!1.00 E+00 (1.0E+0) atm, 300−1800 K, 18% err, 1.00 × N2
PN-2QJ ⇔ PN-2Q4J	6.10×10^{34}	−7.33	26826	!1.00E+00 (1.0E+0) atm, 300−1800 K, 38% err, 1.00 × N2
PN-2QJ ⇔ C(CYOCC)C + OH	4.01×10^{41}	−8.93	43808	!1.00E+00 (1.0E+0) atm, 300−1800 K, 17% err, 1.00 × N2
Dissociation of Stabilized Adduct 2, PN-2Q4J				
PN-2Q4J ⇔ C(CYOCC)C + OH	8.40×10^{19}	−2.79	21393	!1.00E+00 (1.00E+00) atm, 300−1800 K, 7% err, 1.00 × N2
PN-2Q4J ⇔ CH_3CHO + C_3H_6 + OH	10^{12}	0.0	25500	!estimate
Chemical (Double) activation via the Second O_2 Addition to PN-2Q4J				
PN-2Q4QJ + O_2 ⇔ PN-2Q4QJ	2.40×10^{39}	−8.70	7345	!1.00E+00 (1.00E+0) atm, 300−1800 K, 35% err, 1.00 × N2
PN-2Q4QJ + O_2 ⇔ PN-2OJ4QJ + OH	7.71×10^{24}	−3.31	21242	!1.00E+00 (1.00E+0) atm, 300−1800 K, 6% err, 1.00 × N2
PN-2OJ4QJ ⇔ CH_3CHO + C_2O + CH_3CHO	5.0×10^{12}	0.0	6000	!biradicals formation and decomposition
PN-2Q4QJ + O_2 ⇔ PN-2*O4OJ + 2OH	3.41×10^{57}	−14.64	16851	!1.0 E+0 (1.00E+0) atm, 300−1800 K, 17% err, 1.00 × N2
PN-2*O4OJ ⇔ CH_3CHO + CC*OCJ	2. × 10+13	0.0	8000	!estimate
Dissociation of Stabilized Adduct, PN-2Q4QJ				
PN-2Q4QJ ⇔ PN-2OJ4QJ + OH	1.55 × 10+44	−9.23	52172	!1.00E+00 (1.0E+0) atm, 300−1800 K, 21% err, 1.00 × N2
PN-2Q4QJ ⇔ PN-2*O4OJ + 2OH	5.09 × 10+49	−12.44	27034	!1.00E+00 (1.0E+0) atm, 300−1800 K, 52% err, 1.00 × N2

H-bonding feature is retained with the internal (proximal) oxygen atom. At distances near 3.4 Å, the terminal CH_3 undergoes additional rotation to adjust the attachment position. The superposition of these two effects eventually results in the formation of RO_2.

The asymptotic dissociation limit is localized at $\Delta E_\infty \approx 36.5$ kcal mol^{-1}, while ΔE(isolated) = 38.08 kcal mol^{-1}. The difference is likely due to the compensation effects of BSSE destabilizing (∼1.5 kcal mol^{-1}) and H-bonding stabilizing energy errors at close to asymptotic limit geometries. The dissociation reaction enthalpy is ΔH_{298} = 34.81 kcal mol^{-1}, while ΔE(el+zpe) = 33.48 kcal mol^{-1}.

Figure 15 shows a graph for synchronized interactions of the attacking oxygen molecule with the radical center localized initially on the C(1) atom of the 2-propyl radical and represented by the O(1)−C(1) distance (see the inset in Figure 14) and a hydrogen atom via the H···OO distance versus the relative dissociation energy of PR-O_2 (relaxed scan results are in Figure 14).

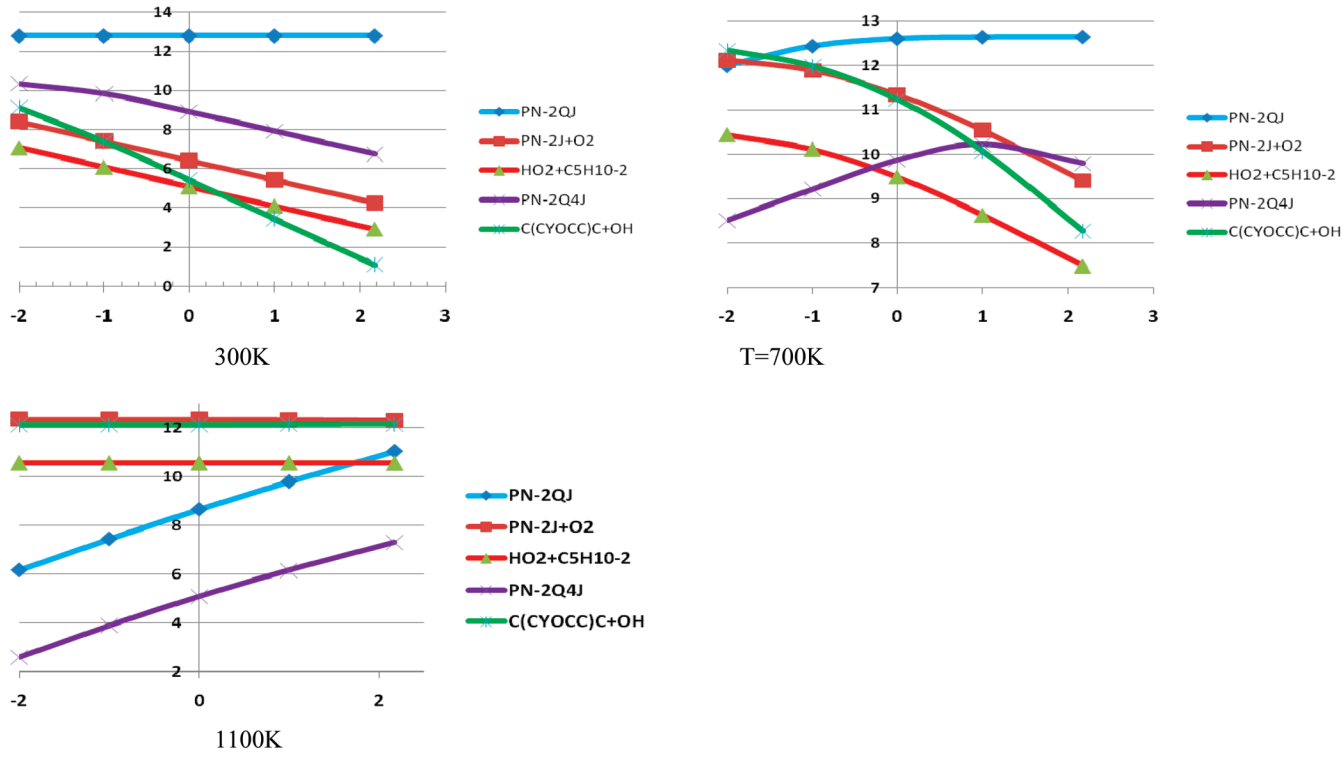

Figure 16. Pressure dependence for first oxygenation of the PN-2J radical.

The peroxy radical H bond between terminal O and H atoms (energy level at the point 0 on the highlighted curve) becomes stronger at 2 Å separation (points 5−7) and remains almost unchanged up to distances of ∼5 Å for terminal and ∼4 Å for central O atoms to C1 (points 38−39), where the H bonding gradually starts to break down. The crossing and interplay of two O−C distances takes place at ∼3.5 Å separation (point 20−22) at almost equal distances. Comparative results at B3LYP/6-311+(2d,p) and QCISD(T)/6-311+(2d,p) levels show similar trends.

Appendix 3

Input high-pressure rate constants and transport properties for the QRRK/master equation calculations are presented in Table A2.

Appendix 4

Selected rate parameters are presented in Table A3.

Appendix 5

Pressure dependence plots are presented in Figure 16 .

Supporting Information Available: Cartesian coordinates for optimized stationary points on respective PESs are tabulated in Tables S1 and S2. This material is available free of charge via the Internet at http://pubs.acs.org.

References and Notes

(1) (a) Bozzelli, J. W.; Dean, A. M. *J. Chem. Phys.* **1993**, *97*, 4427. (b) Bozzelli, J. W.; Sheng, C. Y. *J. Phys. Chem. A* **2002**, *106*, 1113. (c) Sheng, C. Y.; Bozzelli, J. W.; Dean, A. M.; Chang, A. Y. *J. Phys. Chem. A* **2002**, *106*, 7276. (d) Bozzelli, J. W.; Chen, C.-C. 4th Joint Meeting of the U.S. Sections Combustion Institute, Philadelphia, PA, 2005; p C30/1.

(2) (a) Pitz, W. J.; Westbrook, C. K. *Combust. Flame* **1986**, *63*, 113. (b) Westbrook, C. K. *Proc. Combust. Inst.* **2000**, *28*, 1563.

(3) (a) Ignatyev, I. S.; Xie, Y.; Allen, W. D.; Schaefer, H. F., III. *J. Chem. Phys.* **1997**, *107*, 141. (b) Reinstra-Kiracofe, C.; Allen, W. D.; Schaefer, H. F., III. *J. Phys. Chem. A* **2000**, *104*, 9823.

(4) (a) Vedeneev, V. I.; Chernysheva, A. V. *Kinet. Katal.* **1996**, *37*, 469. (b) Chan, W. T.; Hamilton, I. P.; Pritchard, H. O. *J. Chem. Soc., Faraday Trans.* **1998**, *94*, 2303.

(5) (a) DeSain, J. D.; Klippenstein, S. J.; Miller, J. A.; Taatjes, C. A. *J. Phys. Chem. A* **2003**, *107*, 4415. (b) Estupinan, E. G.; Klippenstein, S. J.; Taatjes, C. A. *J. Phys. Chem. B* **2005**, *109*, 8374. (c) Estupinan, E. G.; Smith, J. D.; Tezaki, A.; Klippenstein, S. J.; Taatjes, C. A. *J. Phys. Chem. B* **2007**, *111*, 4015. (d) Miller, J. A.; Klippenstein, S. J. *Int. J. Chem. Kinet.* **2001**, *33*, 654. (e) DeSain, J. D.; Taatjes, C. A.; Miller, J. A.; Klippenstein, S. J. *Faraday Disc.* **2001**, *119*, 101–120.

(6) Carstensen, H. H.; Naik, C. V.; Dean, A. M. *J. Phys. Chem. A.* **2005**, *109*, 2264.

(7) Merle, J. K.; Hayes, C. J.; Zalyubovsky, S. J.; Glover, B. J.; Miller, T. A.; Hadad, C. M. *J. Phys. Chem. A* **2005**, *109*, 3637.

(8) Zhu, L.; Bozzelli, J. W.; Kardos, L. M. *J. Phys. Chem. A* **2007**, *111*, 6361.

(9) Wijaya, C. D.; Sumathi, R.; Green, W. H., Jr. *J. Phys. Chem. A* **2003**, *107*, 4908.

(10) Bozzelli, J. W.; Asatryan, R.; Montgomery, C. J. *Pressure Dependent Mechanism for H/O/C(1) Chemistry*; 5th U.S. Combustion Meeting, San Diego, CA, 2007.

(11) Androulakis, I. P.; Grenda, J. M.; Barckholtz, T. A.; Bozzelli, J. W. *AIChE J.* **2006**, *52*, 3246.

(12) Pfaendtner, J.; Yu, X.; Broadbelt, L. J. *J. Phys. Chem. A* **2006**, *110*, 10863.

(13) Andersen, A.; Carter, E. A. *J. Phys. Chem. A* **2003**, *107*, 9463.

(14) Ogura, T.; Miyoshi, A.; Koshi, M. *Phys. Chem. Chem. Phys.* **2007**, *9*, 5133.

(15) (a) Westbrook, C. K.; Pitz, W. J.; Thornton, M. M.; Malte, P. C. *Combust. Flame* **1988**, *72*, 45–62. (b) Ribaucour, M.; Minetti, R.; Sochet, L. R.; Curran, H. J.; Pitz, W. J.; Westbrook, C. K. *Proc. Combust. Inst.* **2000**, *28*, 1671–1678.

(16) Chakir, A.; Belliman, M.; Boettner, J. C.; Cathonnet, M. *Combust. Sci. Technol.* **1991**, *77*, 239–60.

(17) Minetti, R.; Rouboud, A.; Therssen, E.; Ribaucour, M.; Sochet, R. *Combust. Flame* **1999**, *118*, 213–220.

(18) Zhukov, V. P.; Sechenov, V. A.; Starikovskii, A. Yu. *Combust. Flame* **2005**, *140*, 196–203.

(19) Van Sickle, D. E.; Mill, T.; Mayo, F. R.; Richardson, H.; Gould, C. W. *J. Org. Chem.* **1973**, *38*, 4435–4440.

(20) (a) Asatryan, R.; Bozzelli, J. W. Eastern States Section Combust Inst. Meeting, Charlottesville, Virginia, 2007. (b) Bozzelli, J. W.; Asatryan, R.; Montgomery, C. 235th ACS National Meeting, New Orleans, LA, 2008.

(c) Asatryan, R.; Bozzelli, J. W. 20th International Symposium on Gas-Kinetics, Manchester, U.K., 2008. (d) Asatryan, R.; Bozzelli, J. W. 32nd Int'l Symp. on Combust., Montreal, Canada, 2008.

(21) Fernandes, R. X.; Zador, J.; Jusinski, L. E.; Miller, J. A.; Taatjes, C. A. *Phys. Chem. Chem. Phys.* **2009**, *11*, 1320–1327.

(22) (a) Beck, A. D. *J. Chem. Phys.* **1993**, *98*, 5648. (b) Lee, C.; Yang, W.; Parr, R. G. *Phys. Rev. B* **1988**, *37*, 785.

(23) Montgomery, J. A., Jr.; Frish, M. J.; Ochterski, J. W.; Petersson, G. A. *J. Chem. Phys.* **1999**, *110*, 2822.

(24) Knyazev, V. D.; Slagle, I. R. *J. Phys. Chem. A.* **1998**, *102*, 1770.

(25) (a) Asatryan, R.; Bozzelli, J. W.; Simmie, J. M. *Int. J. Chem. Kinet.* **2007**, *39*, 378. (b) Asatryan, R.; Bozzelli, J. W. *Phys. Chem. Chem. Phys.* **2008**, *10*, 1769. (c) Henry, D. J.; Parkinson, C. J.; Radom, L. *J. Phys. Chem. A* **2002**, *106*, 7927. (d) Kuwata, K. T.; Valin, L. C.; Converse, A. D. *J. Phys. Chem. A* **2005**, *109*, 10710. (e) Gomez-Balderas, R.; Coote, M. L.; Henry, D. J.; Radom, L. *J. Phys. Chem. A* **2004**, *108*, 2874. (f) Guner, V.; Khuong, K. S.; Leach, A. G.; Lee, P. S.; Bartberger, M. D.; Houk, K. N. *J. Phys. Chem. A* **2003**, *107*, 11445. (g) Kuwata, K. T.; Hasson, A. S.; Dickinson, R. V.; Petersen, E. B.; Valin, L. C. *J. Phys. Chem. A* **2005**, *109*, 2514. (h) Coote, M. L. *J. Phys. Chem. A* **2004**, *108*, 3865. (I) Vandeputte, A. G.; Sabbe, M. K.; Reyniers, M.-F.; Speybroyeck, V. V.; Waroquier, M.; Marin, G. B. *J. Phys. Chem. A* **2007**, *111*, 11771 A systematic overestimate for intermolecular H-transfer barriers by ~0.5 kcal mol^{-1} at the CBS-QB3 level compared to that of W1 model chemistry is in fact within the error bars of both current theories and experiments.

(26) Frisch, M. J.; Trucks, G. W.; Schlegel, H. B.; Scuseria, G. E.; Robb, M. A.; Cheeseman, J. R.; Montgomery, J. A., Jr.; Vreven, T.; Kudin, K. N.; Burant, J. C.; Millam, J. M.; Iyengar, S. S.; Tomasi, J.; Barone, V.; Mennucci, B.; Cossi, M.; Scalmani, G.; Rega, N.; Petersson, G. A.; Nakatsuji, H.; Hada, M.; Ehara, M.; Toyota, K.; Fukuda, R.; Hasegawa, J.; Ishida, M.; Nakajima, T.; Honda, Y.; Kitao, O.; Nakai, H.; Klene, M.; Li, X.; Knox, J. E.; Hratchian, H. P.; Cross, J. B.; Bakken, V.; Adamo, C.; Jaramillo, J.; Gomperts, R.; Stratmann, R. E.; Yazyev, O.; Austin, A. J.; Cammi, R.; Pomelli, C.; Ochterski, J. W.; Ayala, P. Y.; Morokuma, K.; Voth, G. A.; Salvador, P.; Dannenberg, J. J.; Zakrzewski, V. G.; Dapprich, S.; Daniels, A. D.; Strain, M. C.; Farkas, O.; Malick, D. K.; Rabuck, A. D.; Raghavachari, K.; Foresman, J. B.; Ortiz, J. V.; Cui, Q.; Baboul, A. G.; Clifford, S.; Cioslowski, J.; Stefanov, B. B.; Liu, G.; Liashenko, A.; Piskorz, P.; Komaromi, I.; Martin, R. L.; Fox, D. J.; Keith, T.; Al-Laham, M. A.; Peng, C. Y.; Nanayakkara, A.; Challacombe, M.; Gill, P. M. W.; Johnson, B.; Chen, W.; Wong, M. W.; Gonzalez, C.; Pople, J. A. *Gaussian 03*, revision D.01; Gaussian, Inc.: Pittsburgh, PA, 2003.

(27) (a) Dean, A. M. *J. Phys. Chem.* **1985**, *89*, 4600. (b) Chang, A. Y.; Bozzelli, J. W.; Dean, A. M. *Z. Phys. Chem.* **2000**, *214*, 1533. (c) Sheng, C. Ph.D. Dissertation, New Jersey Institue of Technology, 2002.

(28) Pfahl, U.; Fieweger, K.; Adomeit, G. *Proc. Combust. Inst.* **1996**, *26*, 781.

(29) Asatryan, R., Bozzelli, J. W., Sumathy Raman, Farrell, J. T. Detailed Chemical Kinetic Mechanism for Combustion of n-Decane. *Proceedings of the 6th U.S. National Combustion Meeting*, Ann Arbor, MI, 2009.

(30) Kurman, M. S.; Natelson, R. H.; Cernansky, N. P.; Miller, D. L. New Methodology for Jet Fuel Surrogate Oxidation and Intermediate Speciation in the Low Temperature Regime. *Proceedings of the 6th U.S. National Combustion Meeting*, Ann Arbor, MI, 2009.

(31) Maranzana, A.; Ghigo, G.; Tonachini, G. *Chem.—Eur. J.* **2003**, *9*, 2616–2626.

(32) Dahlke, E. E.; Truhler, D. G. *J. Phys. Chem. B* **2005**, *109*, 15677.

JP101159H